NASA TECHNICAL NOTE

NASA TN D-3067

C.1

NASA TN D-3067

ELASTIC AND INELASTIC SCATTERING OF 40-MeV ALPHA PARTICLES FROM EVEN TIN ISOTOPES

by Norton Baron, Regis F. Leonard,
John L. Need, and William M. Stewart

Lewis Research Center
Cleveland, Ohio

NATIONAL AERONAUTICS AND SPACE ADMINISTRATION • WASHINGTON, D. C. • OCTOBER 1965

ERRATA

NASA Technical Note D-3067

Completed
MD
10-22-66

ELASTIC AND INELASTIC SCATTERING OF 40-MeV ALPHA

PARTICLES FROM EVEN TIN ISOTOPES

by Norton Baron, Regis F. Leonard, John L. Need, and William M. Stewart
October 1965

Page 2: Before line 1 the following should be added:
scattering leading to excitation of final nuclear states of collective nature; (d) remarkable

Page 12: After the last line the following should be added:
^{120}Sn, and ^{122}Sn. These angular distributions are pictured in figures 4, 5, 6, and 7, respectively.

Page 14: The values of Q in the key in figure 4 should be -1.287 and -2.325 MeV.

NASA-Langley, 1966

Issued 1-28-66

ELASTIC AND INELASTIC SCATTERING OF 40-MeV ALPHA PARTICLES FROM EVEN TIN ISOTOPES

By Norton Baron, Regis F. Leonard, John L. Need, and William M. Stewart

Lewis Research Center
Cleveland, Ohio

NATIONAL AERONAUTICS AND SPACE ADMINISTRATION

For sale by the Clearinghouse for Federal Scientific and Technical Information
Springfield, Virginia 22151 – Price $2.00

ELASTIC AND INELASTIC SCATTERING OF 40-MeV ALPHA PARTICLES FROM EVEN TIN ISOTOPES

by Norton Baron, Regis F. Leonard, John L. Need, and William M. Stewart

Lewis Research Center

SUMMARY

Angular distributions were measured for alpha elastic and inelastic scattering by isotopically enriched targets of ^{116}Sn, ^{118}Sn, ^{120}Sn, and ^{122}Sn using the 40-MeV alpha beam of the NASA 60-inch cyclotron. In each isotope, only two strongly excited states were observed. Their energies were about 1.2 and 2.4 MeV above the ground state.

The elastic angular distributions were analyzed using both the Blair-Fraunhofer black-disk method and the optical model. These analyses are consistent with the concept that the elastically scattered particles result from surface reactions of a direct nature.

The inelastically scattered groups of alpha particles were analyzed using a distorted waves Born approximation (DWBA). The results of these calculations predict the first excited state of each isotope to have a spin of two and positive parity. Similarly, the second excited state of each isotope is predicted to have a spin of three and negative parity. In addition, the angular distributions of the ground state, first excited state, and second excited state of each isotope are observed to obey the Blair phase rule.

Deformation parameters were extracted from the DWBA calculations and are found to be in agreement with those obtained by Coulomb excitation experiments.

INTRODUCTION

An effective tool for studying collective modes of nuclear excitation, as well as the mechanism of direct interaction processes, is the inelastic scattering of medium-energy alpha particles.

The angular distributions of elastically and inelastically scattered alpha particles (or, more generally, strongly absorbed projectiles) have been found to exhibit distinct empirical features: (a) strong peaking in the forward direction; (b) sharp diffraction-like patterns with regular spacing between the successive peaks; (c) enhancement of inelastic scattering leading to excitation of final nuclear states of collective nature; (d) remarkable similarity in shape and simple phase relations between angular distributions for elastic and inelastic scattering.

It was shown by Blair (ref. 1) that these well defined features can be accounted for theoretically in a direct interaction model which assumes the target nucleus to be "black" to the incoming projectiles (i. e., completely absorbing) and which evaluates the scattering amplitude in the adiabatic approximation (i. e., the period of time associated with the nuclear collective motion is considered long compared to the transit time of the projectile).

A particularly significant result of the Blair-Fraunhofer treatment is the familiar "phase rule", which states that the oscillations of an inelastic angular distribution are out of phase (in phase) with those of the elastic angular distribution when the parity change of the target nucleus is even (odd). In addition, it predicts at very forward angles, unique shapes of the angular distributions for different collective modes of nuclear surface excitations without resort to digital computers. However, it does not account for the experimentally observed rapid decrease of cross section with increasing scattering angle and gives, at best, an uncertain value of the nuclear deformation parameter, β_l.

An alternative form of analysis is the theory of direct reactions (refs. 2 to 5). The motion of the projectile relative to the target nucleus is described by the distorted waves calculated for elastic scattering from an optical interaction potential. This type of calculation carried out in the Born approximation is known as a distorted waves Born approximation (DWBA) calculation. Deformations derived from the optical potential used to describe the elastic scattering are treated as perturbations which cause transitions between different elastic scattering states, thus inducing inelastic scattering to final collective states of the nucleus. For (α, α') an expansion for a nonspherical potential well is used, and the interaction is limited to the surface. As in the Blair model, the differential cross section is a product of a factor proportional to β_l^2 and an angular function dependent on the momentum transfer. Since the DWBA calculation (necessitating the use of digital computers) is somewhat more realistic than the Blair treatment, the irregularities in the angular distributions are more pronounced and permit unique spin assignments to be made more readily. In addition, the decrease of cross sections with increasing angle is well reproduced, thus allowing the determination of β_l more accurately than is possible with the Blair model.

To test the validity of the Blair phase rule and the applicability of DWBA calculations to determine the deformation parameter, 40-MeV alpha particles were scattered from the even tin isotopes. The selection of tin was based on three considerations: first, there are a large number of stable tin isotopes; second, since tin possesses a closed proton shell, it is of particular interest to theoreticians; third, the scattering of medium-energy alpha particles had not been done in the tin region.

SYMBOLS

A	nuclear mass number
A_l	strength of l'th component of transition amplitude
a	diffuseness parameter in Woods-Saxon potential
$B(E,l)\uparrow$	reduced transition probability for transition from ground state to an excited state by means of electric 2^l-pole radiation
E_1	energy of incident particle
E_3	energy of light scattered particle
E^*	excitation energy of a level taken with respect to ground state of nucleus
e	unit of electric charge
$f(r)$	form factor of real part of nuclear optical potential
$f(\theta)$	the scattering amplitude
$f_c(\theta)$	Coulomb scattering amplitude
$g(r)$	form factor of imaginary part of nuclear optical potential
$\hbar$	Planck's constant divided by 2π
I	quantum number for intrinsic angular momentum of the nucleus
J	quantum number for total angular momentum
$J_n(x)$	ordinary Bessel function of order n
k	linear momentum in units of $\hbar$
M	quantum number for Z component of total angular momentum
M_1	mass of incident particle in AMU
M_2	mass of target particle in AMU
M_4	mass of residual particle in AMU
m	quantum number for Z component of orbital angular momentum
mb	a unit of area equal to 10^{-27} cm^2
N_l	normalization factor
$P_l(\cos\theta)$	Legendre polynomial of order l
Q	excess of final kinetic energy over initial kinetic energy in nuclear reaction

R	nuclear radius
$R_{Fraunhofer}$	nuclear radius within which the nucleus is totally absorbing
R_o	mean radius of nuclear potential and thus the mean interaction radius
r	semiclassical interaction radius
r_o	distance measured from center of nucleus
T_{fi}	transition amplitude from state i to state f
U	average optical potential
V	strength of real part of nuclear optical potential, MeV
V_c	Coulomb potential
v_f	wave function of final nuclear state
v_i	wave function of initial nuclear state
W	strength of imaginary part of nuclear optical potential, MeV
$Y_l^m(\theta, \Phi)$	spherical harmonic of order l, m
Z	defined in equations (19) to (23)
$\langle J_f M_f \| J_i l M_i m \rangle$	a Clebsch-Gordon coefficient
α, α'	alpha particle
β	nuclear deformation parameter
δ_l	nuclear phase shift for l^{th} partial wave
δ^{lm}	form factor of transition amplitude for angular momentum l with Z component m
η	Coulomb parameter
θ	scattering angle of a reaction product particle in laboratory system
θ_{cm}	scattering angle of a reaction product particle in center of mass system
μ	reduced mass $M_1M_2/(M_1 + M_2)$
π	parity of a nuclear state
σ_R	total reaction cross section
σ_l	Coulomb phase shift
σ_{ex}	experimental differential cross section

σ_{ex}	experimental differential cross section
σ_{th}	theoretical differential cross section
$\Delta\sigma_{ex}$	estimated error in σ_{ex}
$d\sigma/d\Omega$	differential cross section
χ^2	a measure of statistical goodness of fit
Ψ	total wave function

Subscripts:

DWBA	distorted wave Born approximation
f	final state
i	initial state
l	quantum number assigned to orbital angular momentum
m	quantum number assigned to Z component of orbital angular momentum
SP	single particle

EXPERIMENTAL ARRANGEMENT

General

The external 40 MeV alpha-particle beam of the National Aeronautics and Space Administration cyclotron was used in this experiment in conjunction with a 64-inch-diameter scattering chamber. A schematic diagram of the external beam system is shown in figure 1. The deflected beam is magnetically focused onto slit 1. The acceptance angle into the analyzing magnet is controlled by slit 2 placed in front of the magnet. The beam is brought to a focus at slit 5, placed 8 inches in front of the target. The energy spread of the beam incident on the target is controlled by slit 1 (the source slit) and slit 5 (the effective target slit). Slits 3 and 4 serve as scraping slits.

The 64-inch scattering chamber is equipped with a Faraday cup, two movable concentric rings on each of which is mounted a detector arm, and a target-changing and-holding device. The detector arms and target changer can be independently positioned by remote control.

The detector used in the experiment was a windowless lithium-drift silicon semiconductor counter having a compensated depth of 1000 microns. It was operated at room temperature at a bias of about 100 volts with a leakage current of about 1 microampere. Reaction product particles entered the detector through an aperture placed directly in

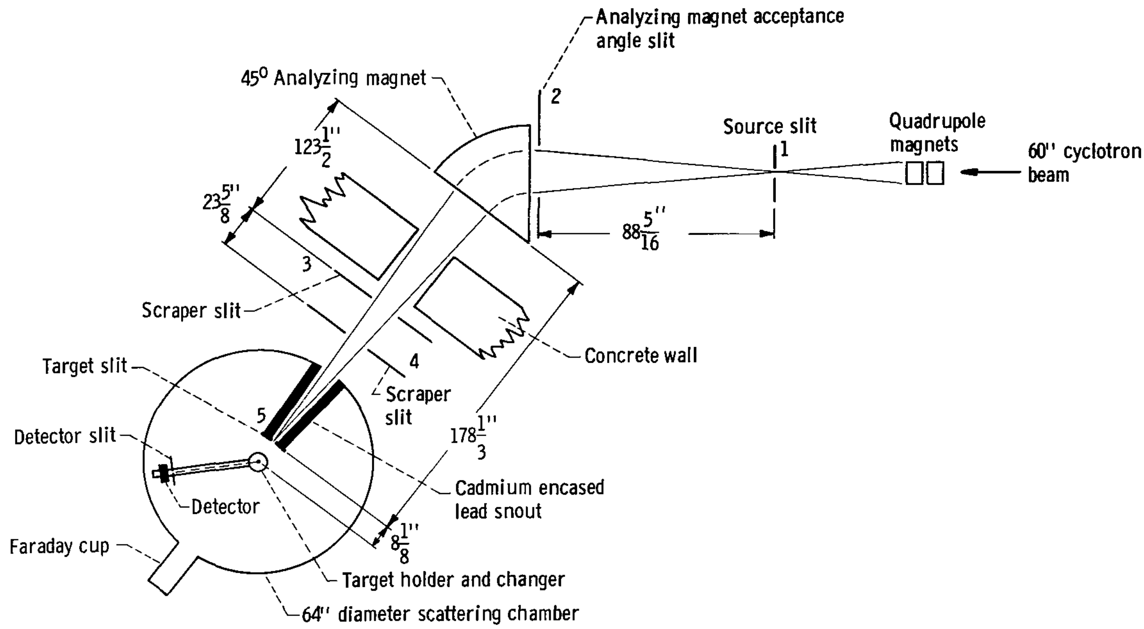

Figure 1. - Experimental scattering system.

front of the detector.

After passing through the target, the beam was stopped in the Faraday cup which consists of a copper cylinder ($5\frac{1}{8}$ in. diam by $12\frac{1}{2}$ in. long) with an air-cooled base of tantalum brazed to copper. The tantalum base of the cup is $55\frac{1}{2}$ inches from the target. Positioned in front of the cup was a brass suppressor ring ($5\frac{1}{8}$ in. diam by 6 in. long). The charge carried into the cup was monitored by a charge integrator, which was carefully calibrated several times during the experiment.

The general characteristics of the scattering system are further illustrated by the following numbers:

The detector angle was known to better than ±0.06 degree.

The target angle was known to ±1.0 degree absolutely and ±0.06 degree relatively.

The angular acceptance of the detector in the scattering plane (for a point source on the target) was 0.5 degree.

The lateral position of slit 1 and the field of the analyzing magnet were always maintained at fixed values during the experiment. Consequently, the average energy of the beam in the scattering chamber was very nearly the same for different runs.

Electronics

A block diagram of the electronics setup is pictured in figure 2. The pulse from

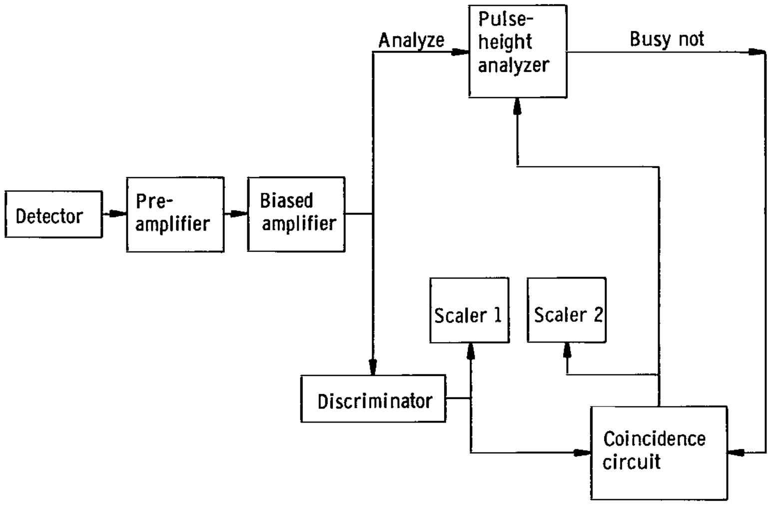

Figure 2. - Block diagram of electronics.

the detector was fed into a low-noise, charge-sensitive preamplifier which was followed by a biased amplifier. The output pulses from the biased amplifier were than fanned out into a 1024-channel pulse-height analyzer (PHA) set to its coincidence mode, and an integral discriminator. The discriminator output pulses fed a scaler and a coincidence circuit. The other input to the coincidence circuit was the "not busy" signal from the PHA. The output of the coincidence circuit drove a second scaler and the coincidence input of the PHA. The ratio of the number of counts in the two scalers served as an analyzer dead-time correction to the cross-section data accumulated in the PHA. During the experiment reported here the counting rate was kept below 100 counts per second except at angles forward of about 30 degrees. Dead-time corrections were made on all runs.

Particle Discrimination

The lithium-drift silicon detector was 1000 microns thick. The maximum energy which an alpha particle can dissipate in this detector is 53 MeV. For other charged particles, the corresponding energies are 47 MeV for ^{3}He, 21 MeV for tritons, 17.7 MeV for deuterons, and 13.2 MeV for protons. The experiment reported here is concerned with elastic and inelastic scattering of 40-MeV alpha particles in order to investigate states of the residual nucleus with excitation energies between 0 and about 10 MeV. Thus it is necessary that in the portion of the pulse-height spectra corresponding to energies between about 30 and 40 MeV, only pulses of alpha particles should be present. From the quoted energy losses in a 1000-micron-thick detector, no particles except alphas and ^{3}He could contribute to the pulse-height spectra range of interest.

However, since the (α, ^{3}He) reactions on the even tin isotopes have Q values no larger than -13.37 MeV, ^{3}He particles will not appear in the pulse-height spectra range of interest.

Reactions of the type (α, x), where x is a particle heavier than an alpha particle, also do not contribute to the pulse height spectra range of interest since they have large negative Q values due to the large binding energy of the alpha particle.

Thus, all the pulses in the pulse-height spectra range of interest must correspond to alpha particles. These could be either elastic or inelastic alphas from the nucleus being investigated or from contaminant elements in the target. However, the difference between these two sources of alpha scattering may readily be distinguished by observing the kinematic behavior of the peak. Nevertheless, the presence of these background alphas due to target contaminants can result in considerable uncertainties in the measured cross sections.

Measurement of Excitation Energies

The total electronic system was calibrated using the elastic scattering from all the isotopes at a sufficient number of angles to cover the pulse-height region of the inelastic levels as measured for the most forward data. A quadratic equation was fitted to the experimental detector energy against PHA channel number data. The detector energy was calculated from a knowledge of the angle of observation, beam energy, and effective target thickness. The detector energies of the inelastic peaks were obtained from the calibration curve and then used to calculate the excitation energies of the levels. The principal source of error is in the determination of the positions of the several peaks and amounts to ±14 keV in energy. Errors in beam energy and detector angle enter only to second order. The change in E* for a 1 MeV assumed change in incident energy amounted to 1 keV. The measured excitation energies are listed in table III (p. 31).

Energy Resolution

Slit	Width, in.	Height, in.
1	0.040	1.0
2	1.0	1.0
3	.040	2.0
4	.040	2.0
5	.070	.625
Detector slit	.0625	.250

The energy resolution of the scattering experiment (refs. 6 and 7) is determined by the geometry of the slit system, the effects of target thickness and target nonuniformity, the detector and electronics noise, and the gain stability of the amplifier chain and the stability of the analyzing magnet current over the period of time required for a single run.

Geometry of the slit system. - Using the notation of figure 1, typical slit settings are given in the table at the left.

The energy of the outgoing reaction product particle varies with the angle defined by its direction and that of the incident beam. However, the direction of the incident beam is undetermined to the extent of its angular spread at the target which, from figure 1, is readily calculated to be 0.126 degree. Thus, the energy spread resulting from the angular spread of the incident beam at the target is calculated to be 4.1 keV. Similarly, the uncertainty in the direction of the outgoing reaction product particle is 1.2 degrees when the detector slit is 7.7 inches from the target. Thus, the energy spread resulting from the angular spread of the outgoing reaction product particles at the detector is calculated to be 39 keV.

The calculated linear dispersion of the double-focusing wedge-type analyzing magnet is 0.0018 inch per keV at the position of slit 5 and 0.0011 inch per keV at the position of slit 1. Thus the energy spread of the analyzed beam due to the width of slit 1 is calculated to be 36 keV, and the energy spread of the beam due to the width of slit 5 is calculated to be 39 keV.

Target thickness and nonuniformity. - For a given reaction with the target in transmission a target angle can be found for each scattering angle such that there is no effect on resolution due to the uncertainty of the depth within the target at which the reaction occurs. However, there is a contribution to the resolution related to the target thickness due to variations in energy loss of the incident and outgoing particles. This energy-straggle contribution for 40 MeV alpha particles and a 1-milligram-per-square-centimeter-thick tin target is calculated to be 45 keV for scattering in the forward hemisphere.

Detector and electronic noise. - The noise of the electronic system was measured (using a precision pulser) to be less than 10 keV. The overall resolution of the detector-electronic system for a monoenergetic source of 8.78 MeV alpha particles from ^{212}Po was measured to be 35 keV. Thus, it can be concluded that the resolution of the detector-electronic system was essentially unaffected by the electronic noise.

Gain stability. - The gain stability of the system was much better than 0.1 percent for a single run of about 60 minutes.

Overall resolution. - The contributions of the resolution factors discussed in the preceding sections are incoherent, so that the energy spread of the scattering system is the square root of the sum of their squares. Using the above figures, the calculated resolution is found to be 87 keV. This agrees very well with experimental resolutions of 80 keV when the above figures were applicable. However, in order to decrease the data-taking time for small cross sections, the slit widths were opened in order to increase incident beam current. The resultant resolution in such cases was 120 keV.

Beam Energy

The beam energy measurement consisted of finding a pair of scattering angles such that the alpha particles elastically scattered by ^{12}C (a thin polystyrene target) at θ_1 have the same pulse height as the inelastically scattered alphas (Q = -4.433 MeV) scattered at θ_2 (ref. 8). For each pair θ_1, θ_2 the equality can be written

$$E_3(Q = 0, \theta = \theta_1, E_1) = E_3(Q = -4.433, \theta=\theta_2, E_1) \tag{1}$$

where E_1 and E_3 are the energies of the incident and light scattered particle, respectively. The explicit form of the function $E_3(Q, \theta, E_1)$ is obtained from the Q equation where

$$Q = E_3\left(1 + \frac{M_3}{M_4}\right) - E_1\left(1 - \frac{M_1}{M_4}\right) - \frac{2\sqrt{M_1E_1M_3E_3}}{M_4}\cos\theta \tag{2}$$

where M_1 and M_3 are the masses of the incident and reaction product particles, and M_4 is the mass of the residual nucleus. The estimated probable error (±0.25 MeV) associated with this measurement was based on the uncertainty in the scattering angles (±0.06 deg) and in the known value of Q. The result of this measurement indicates that the incident beam energy is 40.00±0.25 MeV.

Cross Sections

Relative cross sections. - In estimating the errors in the measured relative cross sections the following sources of uncertainty were considered:

(1) Background: Background consisted of three types - a broad distribution varying smoothly with energy and only of consequence forward of 45 degrees, low energy tails of intense elastic peaks, and interference from contaminant peaks. For the first two cases, background subtraction was performed by drawing a smooth curve through the background on either side of a peak and continuing under the peak. In the case of interfering peaks from contaminants no data are presented where the peak separations were less than 1.5 times the resolution for the run. For those cases of interference included in the present data the separation was performed by drawing smooth curves that summed to the data points.

(2) Statistical uncertainties in the number of counts in each peak: Normally enough counts were accumulated in each spectrum so that the standard deviation was less than

plus or minus 10 percent except for those cross sections less than 0.01 millibarn per steradian.

(3) Random errors: It was found that the relative cross section corresponding to the maximum of angular distributions for the elastic and strongly excited inelastic groups were always reproducible to within the statistical errors and background errors associated with these cross sections (usually less than 1 percent).

Absolute cross sections. - The major sources of probable error in the established scales of absolute cross sections are associated with (a) the determination of the target thickness at the location of the beam spot, and (b) the determination of the actual number of incident alpha particles for a given amount of measured charge collected by the Faraday cup.

Target thicknesses were measured by a transmission experiment. Alpha particles from a mesothorium source containing ^{212}Bi and ^{212}Po were used. The detector pulses from these groups of alphas were sent through the electronic system and displayed on a pulse-height analyzer (PHA) thereby calibrating the detector system. The target was then moved between the source and detector thereby degrading the energies of the alpha particles before they entered the detector. Since the PHA was calibrated in unit of energy per channel, the decrease in channel number is directly related to the loss of energy. From range-energy tables (ref. 9), the target thickness is readily obtained from the loss of energy. The principal uncertainty in the thickness measurement is the imperfect knowledge of the range-energy relation.

Target	Thickness, mg/cm^2	Isotopic enrichment, percent
^{116}Sn	0.374	95.74
^{118}Sn	6.95	97.15
^{120}Sn	1.22	98.39
^{122}Sn	.955	90.80

The targets used in this experiment were determined to have the thicknesses and isotopic enrichments given in the table at the left. These thicknesses represent an average of five measurements which were located in the region struck by the beam. The isotopic enrichments were furnished by the isotopic materials supplier (i.e., the Oak Ridge National Laboratory Isotopes Development Center).

The Faraday cup and suppressor ring are separated from the scattering chamber by 5-mil aluminum foil in order to utilize a separate pumping system on the cup and achieve a better vacuum in the cup than is possible in the large scattering chamber. An accurate evaluation of the actual number of incident alpha particles (b) requires a thorough investigation of the problems of secondary electron emission in the cup, knockout electrons from the 5-mil aluminum foil covering the entrance into the cup by the passage of the incident beam through the foil, and the ionization of the residual gas in the cup. Simultaneous use of a monitor counter and variation of the suppressor-ring voltage indicated that 1000 volts on the suppressor ring is sufficient to inhibit unwanted electron transfer into or out of the cup.

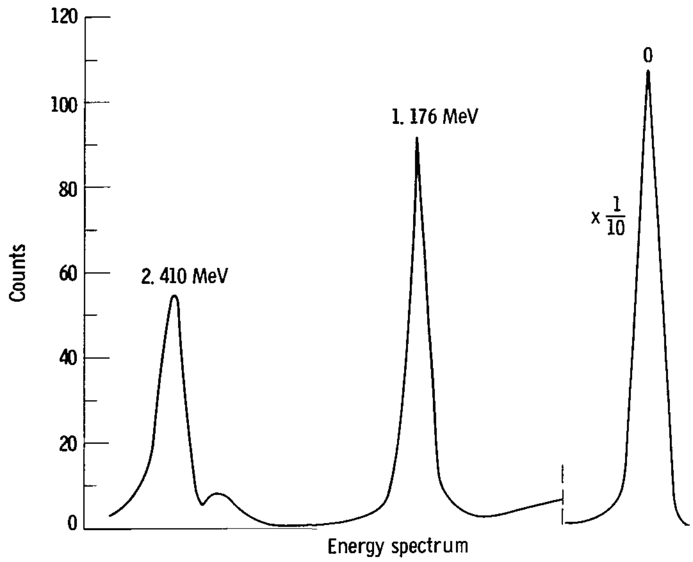

Figure 3. - Typical energy spectrum of scattered alpha particles for ^{120}Sn; scattering angle, 44^{o}.

Small contributions (less than 1 percent of the absolute cross section) to the overall probable error in the absolute scales resulted from the measurement of the acceptance solid angle of the detector. The overall uncertainty in the absolute cross sections was estimated to be less than 7 percent for all the angular distribution measurements reported in this experiment, except for those measurements when statistical uncertainties are dominant.

EXPERIMENTAL CROSS SECTIONS AND THEIR STATISTICAL ERRORS

General

Cross sections were obtained for elastic scattering ($20^{o} < \theta < 150^{o}$) and for the excitation of two strongly excited states ($20^{o} < \theta < 90^{o}$) of each of the four tin isotopes. No other strong excitations were observed. A typical energy spectrum is pictured in figure 3. The upper limit of other alpha inelastic reaction cross sections at 30 degrees is 0.05 millibarn per steradian.

Cross Sections

The experimental differential cross sections (in mb/sr) and their associated statistical counting errors (in mb/sr) are listed in appendix A for scattering by ^{116}Sn, ^{118}Sn, ^{120}Sn, and ^{122}Sn. These angular distributions are pictured in figures 4, 5, 6, and 7, respectively.

THEORY

Introduction

The work discussed in this report involves the inelastic scattering of alpha particles by even tin nuclei leading to the excitation of low-lying collective states. A method for obtaining spectroscopic information (J^{π}) about these collective states from the experimental data is given by the theory of direct reactions. This theory calculates the transition amplitude for the reaction as the matrix element of a perturbation potential between two elastic scattering states. The wave functions for the elastic scattering states are generally taken to be those generated by an optical potential. The optical potentials are chosen by fitting to experimental elastic-scattering cross sections (ref. 10). The perturbation interaction is the interaction between the incoming entity and collective states in the target nucleus. This interaction is described by a parameter β_l which characterizes the nuclear deformation. This calculation is commonly called a DWBA (distorted waves Born approximation). The inelastic cross sections (proportional to the square of the transition amplitudes) are thus proportional to β_l^2 so this method is a sensitive way of determining the nuclear deformation.

In addition, a semiclassical treatment of alpha particle scattering invoking the concepts of the Blair model can many times give useful information about the effective nuclear radius for elastic scattering as well as spectroscopic information when the nucleus is in an excited state.

Optical Model

In the problem of scattering of a nucleon by a nucleus, an exact treatment involving the interaction between the incident particle and all the target particles is a complicated and difficult one. It is hence desirable to devise reasonable approximations which are valid for certain purposes. One such approximation, known as the optical model, or cloudy-crystal-ball model (ref. 11), has been proposed and extensively employed for collisions between a nucleon (or bound aggregate of nucleons such as an alpha particle) and a target nucleus. This model replaces the exact interaction by a central averaged potential of interaction between the target nucleus and the incident particle. This optical potential, consisting of a real and imaginary part, is analogous to the representation in physical optics of the diffraction of light by a spherical medium having a refractive index consisting of a real and imaginary part, where the real part gives the refraction while the imaginary part accounts for the absorption by the medium. Just as the index of refraction for such a medium defines the interaction of light waves not with each individual

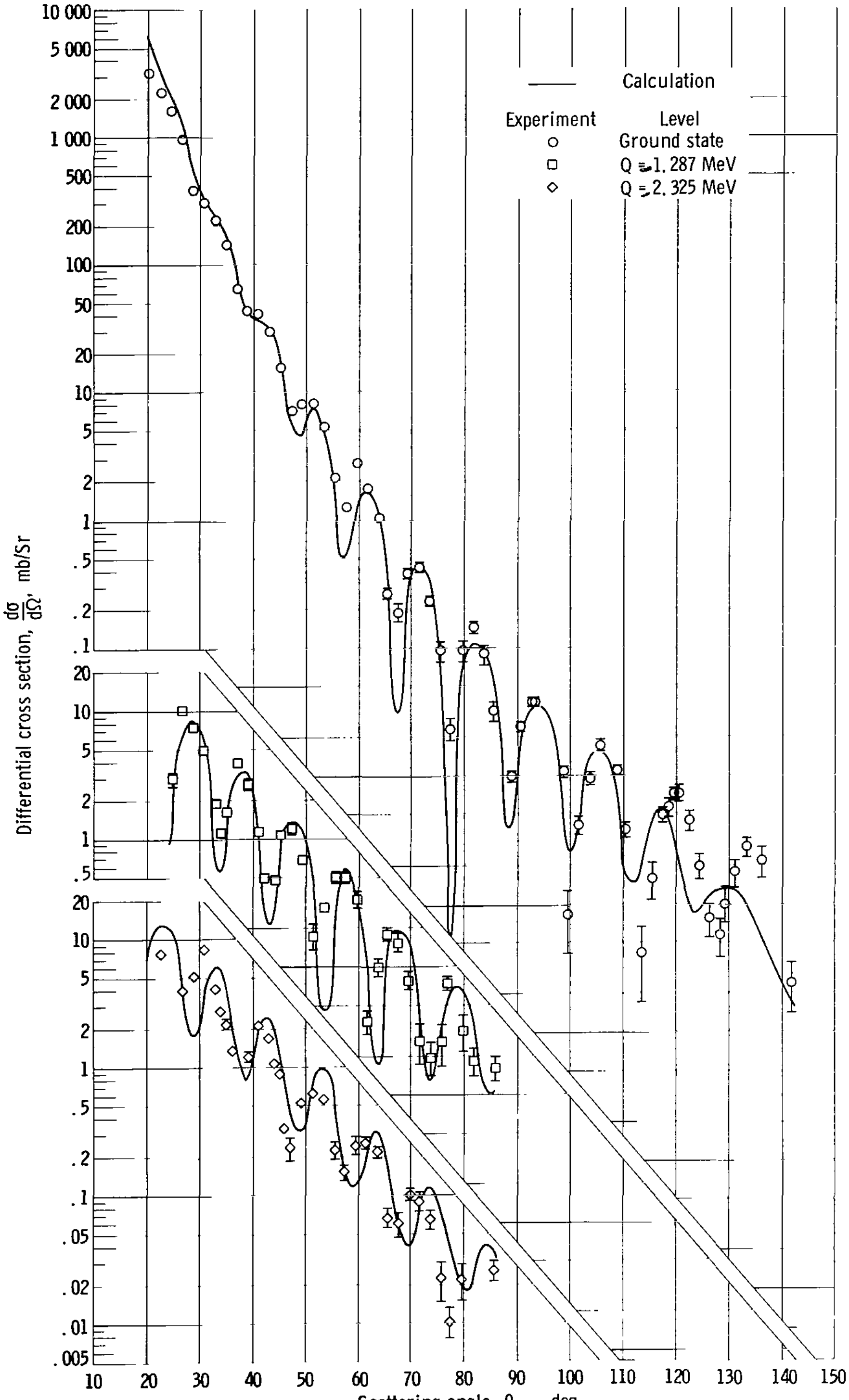

Figure 4. - Elastic and inelastic angular distributions (experimental and calculated) of alpha particles scattered from ^{116}Sn.

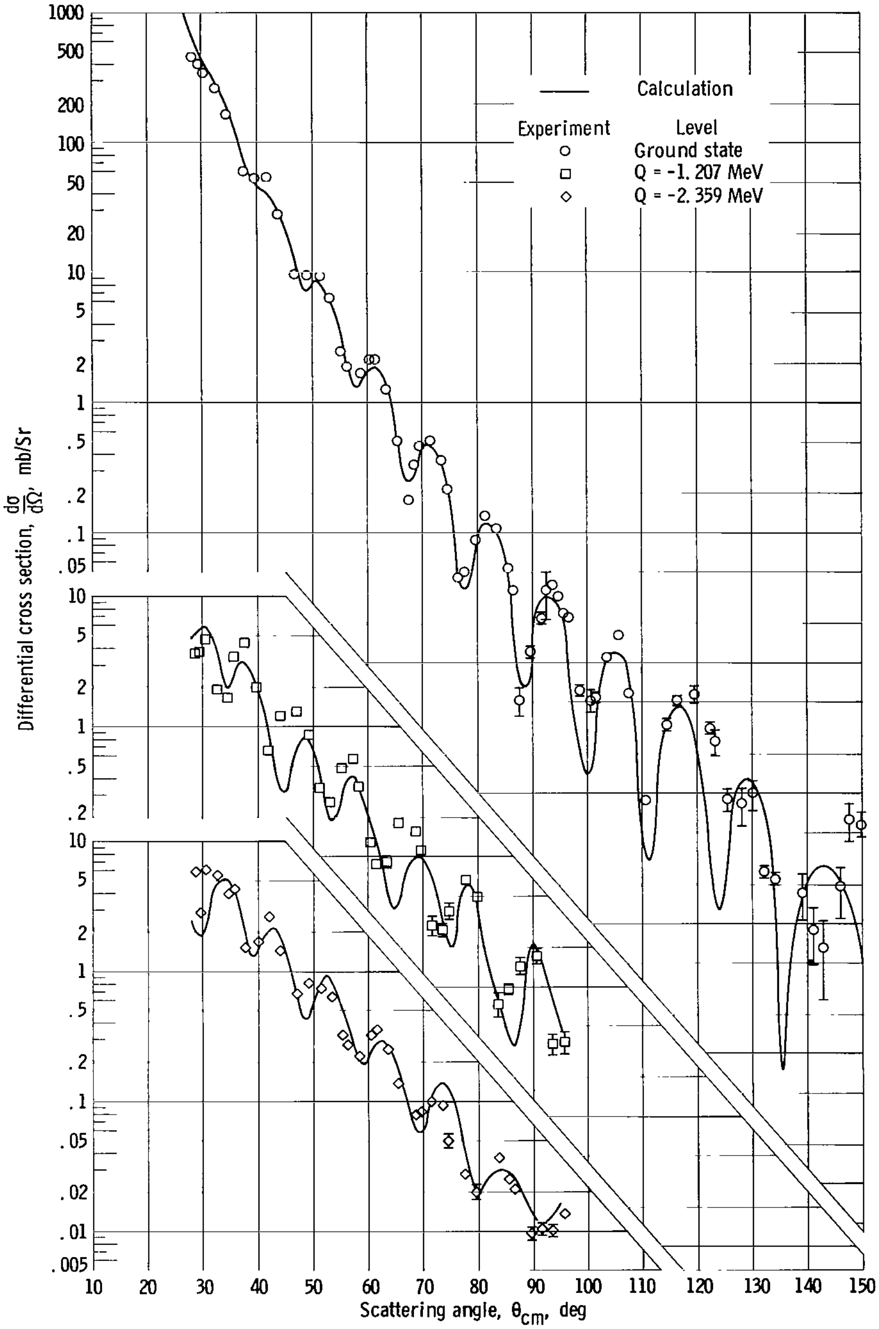

Figure 5. - Elastic and inelastic angular distributions (experimental and calculated) of alpha particles scattered from ^{118}Sn.

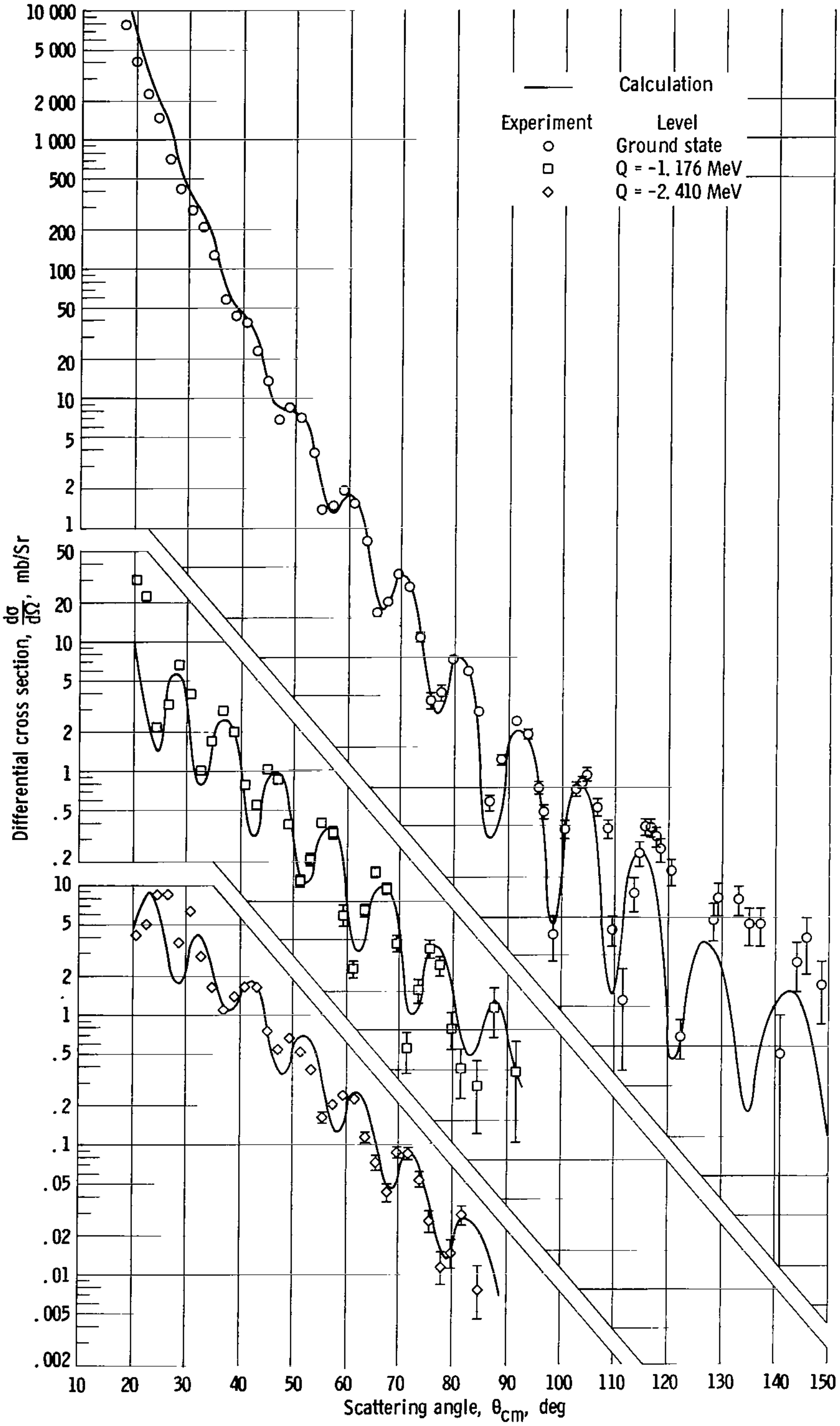

Figure 6. - Elastic and inelastic angular distributions (experimental and calculated) of alpha particles scattered from ^{120}Sn.

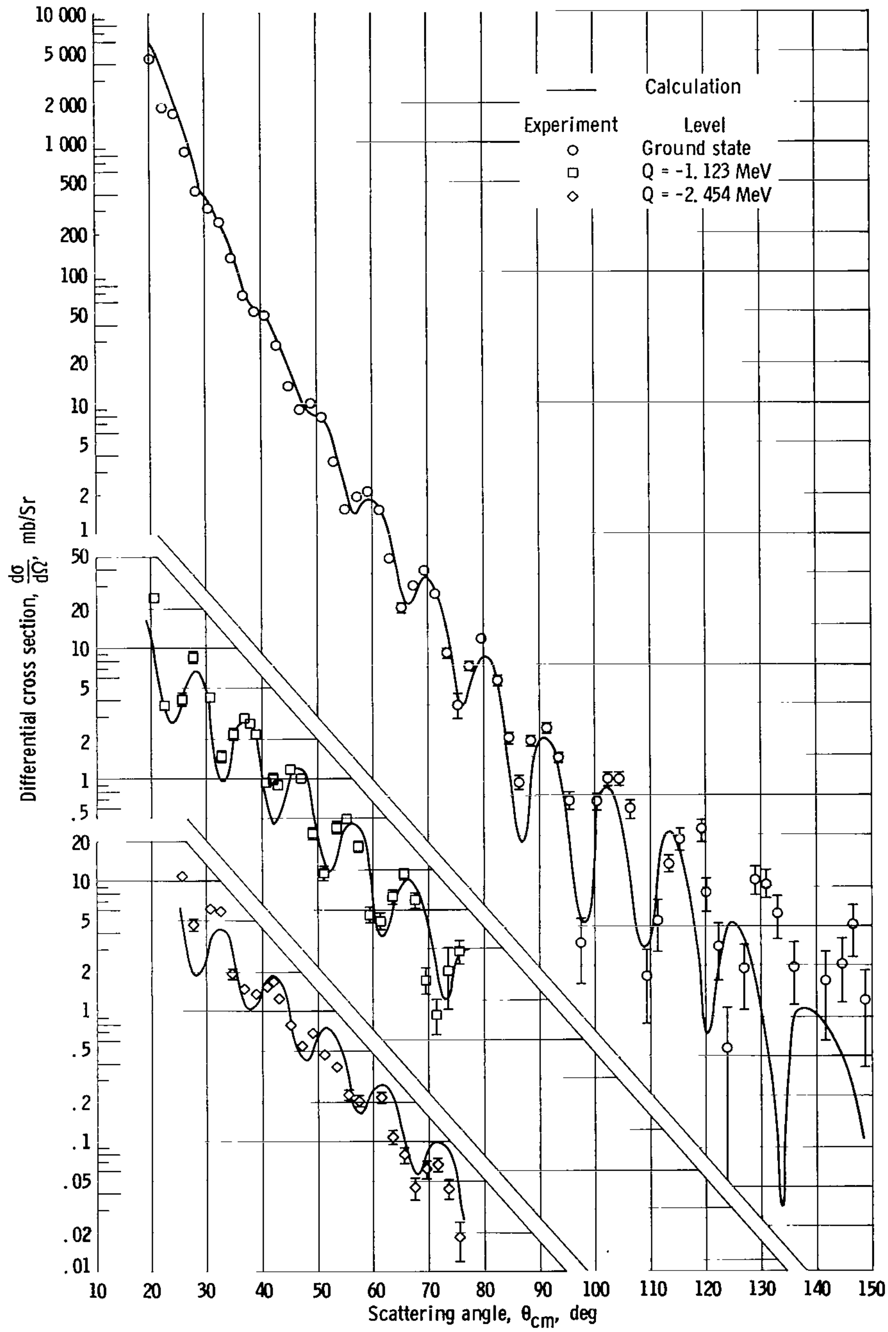

Figure 7. - Elastic and inelastic angular distributions (experimental and calculated) of alpha particles scattered from ^{122}Sn.

electron, but with all of them together, so does the optical-model potential purport to describe the interaction of an incoming nucleon with the average effect of all the nucleons in the target nucleus. It is, of course, an assumption that the scattering of nucleons by complex nuclei is in fact describable by the diffraction of the nucleon's wave by some potential. This, however, is the basic assumption of the optical model. The extent to which this model is useful will be determined by the accuracy with which it can predict observables such as total cross sections and angular distributions for elastic scattering when the dynamical equations of motion are solved with the optical potential.

The optical potential can be written as

$$U(r) = V_c(r) - V \cdot f(r) - iW \cdot g(r) \tag{3}$$

where $V_c(r)$ accounts for the Coulomb electrostatic potential if the incident particle is charged, V and W are the strengths of the real and imaginary parts of the optical potential (accounting for the nuclear scattering and absorption respectively of the incident particles), and $f(r)$ and $g(r)$ are their radial form factors. Since the potential of a nucleon in a nucleus is expected to be uniform in the nuclear interior (due to the short range and saturation character of the nucleon-nucleon forces), fall off in the surface region, and finally drop exponentially to zero, it is convenient to represent the variation analytically by the Woods-Saxon form factor

$$f(r) = g(r) = \frac{1}{1 + \exp\left(\frac{r - R_o}{a}\right)} \tag{4}$$

In this expression, R_o measures the overall extent of the potential and is thus a measure of the nuclear radius. It is usual to put $R_o = r_o A^{1/3}$ where A is the nuclear mass number. The parameter a controls the rapidity with which $f(r)$ falls from its maximum value; it is therefore related to the diffuseness of the nuclear surface.

The measurable quantities such as total cross sections and elastic angular distributions may be calculated from the optical potential by solving the Schrödinger equation

$$\nabla^2\Psi + \frac{2\mu}{\hbar^2}\left[E - U(r)\right]\Psi = 0 \tag{5}$$

subject to the condition that the asymptotic form of the total wave function Ψ is that of an incident plane wave plus a spherical scattered wave. This may be done by expanding Ψ in partial waves

$$\Psi = \sum_{l=0}^{\infty} \frac{\Psi_l(r)}{r} P_l(\cos\theta) \tag{6}$$

and substituting in equation (5) to give the radial wave equation

$$\frac{d^2\Psi_l}{dr^2} + \frac{2\mu}{\hbar^2}\left[E - U(r) - \frac{\hbar^2 l(l+1)}{2\mu r^2}\right]\Psi_l = 0 \tag{7}$$

These equations may be integrated numerically for each value of l contributing to the interaction, and the resulting (complex) radial wave functions are matched to the known asymptotic forms beyond the nuclear field to give the nuclear phase shift δ_l. The angular distributions of the differential cross sections, required observable quantities, are then given by

$$\frac{d\sigma(\theta)}{d\Omega} = \left|f(\theta)\right|^2 \tag{8}$$

where

$$f(\theta) = f_c(\theta) + \frac{1}{2ik}\sum_{l=0}^{\infty} e^{2i\sigma_l}(2l+1)(e^{2i\delta_l} - 1)P_l(\cos\theta) \tag{9}$$

in which $f_c(\theta)$ is the Coulomb scattering amplitude and σ_l is the Coulomb phase shift. The reaction cross section, another required observable quantity, is given by

$$\sigma_R = \frac{\pi}{k^2}\sum_{l=0}^{\infty}(2l+1)\left(1 - \left|e^{2i\delta_l}\right|^2\right) \tag{10}$$

The most laborious part of the calculation is the numerical integration of the radial-wave equations (7), and this has to be done so many times that the use of an electronic computer is essential. The computer program is written so that starting from a given set of parameters of the optical potential (V, W, r_0, a), the computer will automatically optimize specified parameters by iteration to obtain the best fit to a given elastic angular distribution.

In the DWBA formulation of direct reaction theory the inelastic scattering of a particle with incident momentum $\hbar\vec{k}_i$ and final momentum $\hbar\vec{k}_f$ in which the target nucleus is excited from a state v_i to a final state v_f, yields a transition amplitude given by (refs. 3 and 4)

$$T_{fi} = \int d\vec{r}\,\Psi_f^{(-)*}(\vec{k}_f, \vec{r}) < v_f|V|v_i > \Psi_i^{(+)}(\vec{k}_i, \vec{r}) \tag{11}$$

The resulting differential cross section is written as

$$\frac{d\sigma}{d\Omega} = \left(\frac{\mu}{2\pi}\right)^2 \frac{k_f}{k_i} \sum_{av} |T_{fi}|^2 \tag{12}$$

where $\sum_{av}$ means to sum over final states and average over initial states. The $\Psi(\vec{k}, \vec{r})$ are the distorted waves which describe the elastic scattering of the particle by the nucleus before and after the inelastic transition, and are obtained as described in the preceding section. The remaining factor in the transition amplitude is the matrix element of the interaction causing the inelastic transition, taken between the internal states of the colliding pair. It plays the role of an effective interaction for scattering from one elastic scattering state to another, and contains all the information on nuclear structure, angular momentum selection rules, etc.

If this interaction is expanded in terms of multipoles, that is, into a sum of terms each corresponding to a given value of angular momentum, and substituted into the expression for the transition amplitude together with the partial wave expansion of the optical-model wave functions the result can be expressed as

$$T_{fi} = \frac{\sqrt{4\pi}}{k_f^2} \sum_{l} A_l < J_f M_f | J_i l M_i m > \delta^{lm}(\theta) \times (2l + 1)^{1/2} \tag{13}$$

that is, a sum over transition amplitudes (for transfer of angular momentum l z-component m) weighted by Clebsch-Gordon coefficients and a strength A_l. The resulting differential cross section can now be written as

$$\frac{d\sigma}{d\Omega} = \frac{2J_f + 1}{2J_i + 1} \sum_{l} |A_l|^2 \frac{\mu^2}{k_f^3 k_i \pi \hbar^4} \sum_{m} |\delta^{lm}(\theta)|^2 \tag{14}$$

Collective Model Form Factors (refs. 3 and 4)

The collective model of the nucleus attributes many low-lying excited states to oscillations in shape about a spherical mean (vibrations), or to the rotations of a statically deformed shape. This leads naturally to an extension of the optical model to include nonspherical potentials. It is the nonspherical parts of the potential that are presumed to be able to induce inelastic scattering to these collective vibrational or rotational states.

For rotational excitation, the total interaction potential (one with a perturbed shape) is written as a sum of two parts. The first part is the spherical optical potential that produces the elastic scattering and the second is the deviation from sphericity that produces the inelastic transitions. This deviation is expanded in multipole orders and the coefficients of the expansion are given in terms of the deformation parameter β_l and asymmetry parameter of Bohr and Mottelson (ref. 24). For axially symmetric even nuclei the strength A_l has been shown to be directly proportional to the deformation parameter β_l.

For vibrational excitations, the procedure is the same and A_l is again proportional to β_l, which in this case is the root mean square deformation in the ground state due to zero point oscillations.

Blair Model

Another method by which inelastic scattering data can be treated to obtain spectroscopic information is by Blair's generalized "Fraunhofer" treatment of the inelastic diffraction model (ref. 1). The approximations made in this treatment are:

(a) The scattering amplitude is calculated in the adiabatic approximation.

(b) The nucleus is assumed to be strongly absorbing within a sharp radius R defined by

$$R = R_o\left(1 + \sum_{lm} \alpha_{lm} Y_l^m(\theta)\right) \tag{15}$$

where α_{lm} are the collective deformation parameters.

(c) Only terms linear in α are retained in the expansion of the scattering amplitude.

(d) Coulomb effects are neglected.

(e) The Fraunhofer approximation, which is valid for small angles, is used in calculating the scattering amplitudes.

The Fraunhofer model elastic cross section is given by the "black disk" formula

$$\frac{d\sigma}{d\Omega} = (kR_o^2)^2 \left(\frac{J_1(x)}{x}\right)^2 \tag{16}$$

where

$k \equiv$ wave number in center of mass system

$R_o \equiv$ mean interaction radius

$x \equiv 2kR_o \sin \frac{\theta_{cm}}{2}$

$\theta \equiv$ scattering angle in center of mass system

$J_1(x) \equiv$ first-order Bessel function whose argument is x

The general expression for the inelastic scattering cross section can be written as the product of an angular function $Z_l(x)$ and a normalization factor N_l,

$$\frac{d\sigma}{d\Omega}(l, I_i \rightarrow I_f) = N_l Z_l(x) \tag{17}$$

where l is the multipolarity of the collective excitation and I_i, I_f are the initial and final angular momenta of the nucleus.

The normalization factor N_l is given by

$$N_l = \beta_l^2 R_o^2 \tag{18}$$

where β_l is the same parameter discussed in the Collective Model Form Factors section.

The explicit forms of $Z_l(x)$ obtained are listed below for several values of l.

$$l = 0: \quad Z_o(x) = \frac{1}{4\pi}(kR_o)^2\left[J_o(x)\right]^2 \tag{19}$$

$$l = 2: \quad Z_2(x) = \frac{1}{4\pi}(kR_o)^2\left[\frac{1}{4}J_o^2(x) + \frac{3}{4}J_2^2(x)\right] \tag{20}$$

$$l = 3: \quad Z_3(x) = \frac{1}{4\pi}(kR_o)^2\left[\frac{3}{8}J_1^2(x) + \frac{5}{8}J_3^2(x)\right] \tag{21}$$

$$l = 4: \quad Z_4(x) = \frac{1}{4\pi} (kR_o)^2 \left[\frac{9}{64} J_o^2(x) + \frac{20}{64} J_2^2(x) + \frac{35}{64} J_4^2(x)\right] \tag{22}$$

$$l = 5: \quad Z_5(x) = \frac{1}{4\pi} (kR_o)^2 \left[\frac{30}{128} J_1^2(x) + \frac{35}{128} J_3^2(x) + \frac{63}{128} J_5^2(x)\right] \tag{23}$$

These formulas show that for even (or odd) values of l, the Bessel functions are of even (or odd) order. This fact is a result of the restriction $(l + m)$ = even, which occurs in the evaluation of Z. In application, this leads to Blair's phase rule; namely, for transition to single-phonon states, the inelastic distributions of odd momentum transfers are in phase with the elastic distributions and out of phase with inelastic distributions of even momentum transfers. The phase rule is generally stated in terms of parity change since, for collective transitions in the $K = 0$ rotational band, the angular momentum change and parity change are identical.

If $d\sigma/d\Omega$ (elastic) is divided by $k^2R_o^4$ and $\frac{d\sigma}{d\Omega}(l, I_i \rightarrow I_f)$ is divided by

$N_l \frac{(kR_o)^2}{4\pi} \equiv \left(\frac{k^2R_o^4\beta_l^2}{4\pi}\right)$, then the resulting functions are universal in the sense that they depend on k and R_o through the argument x only. The cross sections can therefore be expressed in a "reduced" form which allows for direct comparison to be made among various measurements which may correspond to different values of k or R_o (i.e., different beam energies and/or different target nuclei). These "universal" curves for the elastic and inelastic distributions (l = 2, 3, 4, and 5) are shown in figure 8.

The following method, which corresponds to the simple form of equation (17), was used in the Blair-Fraunhofer analysis of the angular distributions of inelastically scattered alpha particles discussed in this report. The parameter R_o in equation (16) was obtained experimentally by matching the observed positions of the maxima and minima to the predictions of equation (16). Using this value of R_o, a function Z was found which gave the best fit to the locations of the maxima and minima of the observed inelastic angular distribution. The parameter N_l which measures the collective matrix elements involved in the transition was then obtained from equation (17) by normalizing the selected "shape" function $Z_l(x)$ to the observed angular distribution.

A major criticism of the Fraunhofer treatment is that it does not account for the rapid decrease of the differential cross sections observed in nature. As a result, the factors N_l are usually underestimated in the Fraunhofer analysis. It follows that the value of N_l is strongly dependent on the choice of the particular maximum in the oscillatory pattern at which N_l is estimated. Inspection of figure 8 reveals that the angular distributions resulting from angular momentum transfers of 2 and 4 are virtually indis-

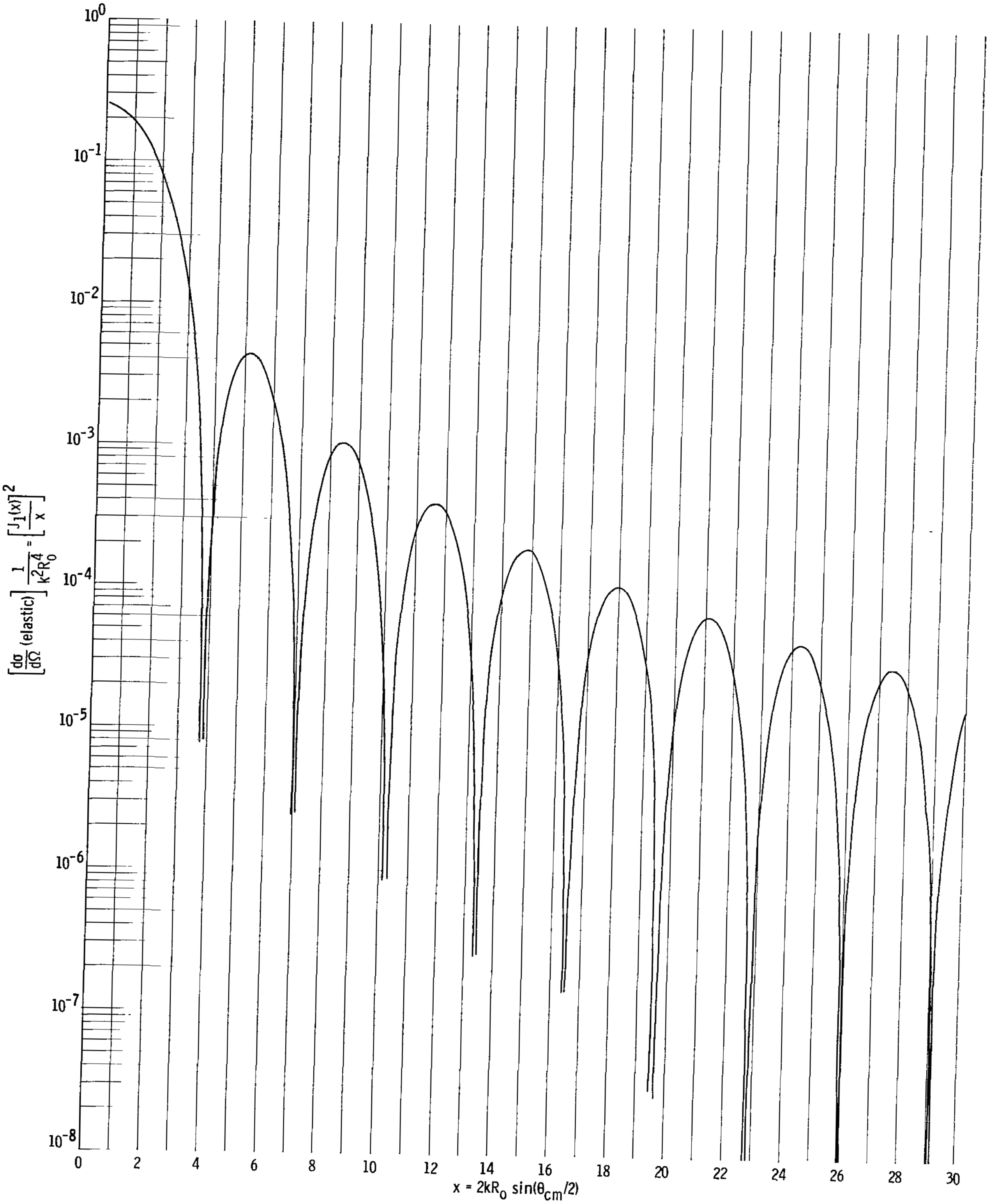

(a) Elastic scattering.

Figure 8. - Angular distributions predicted by Fraunhofer model.

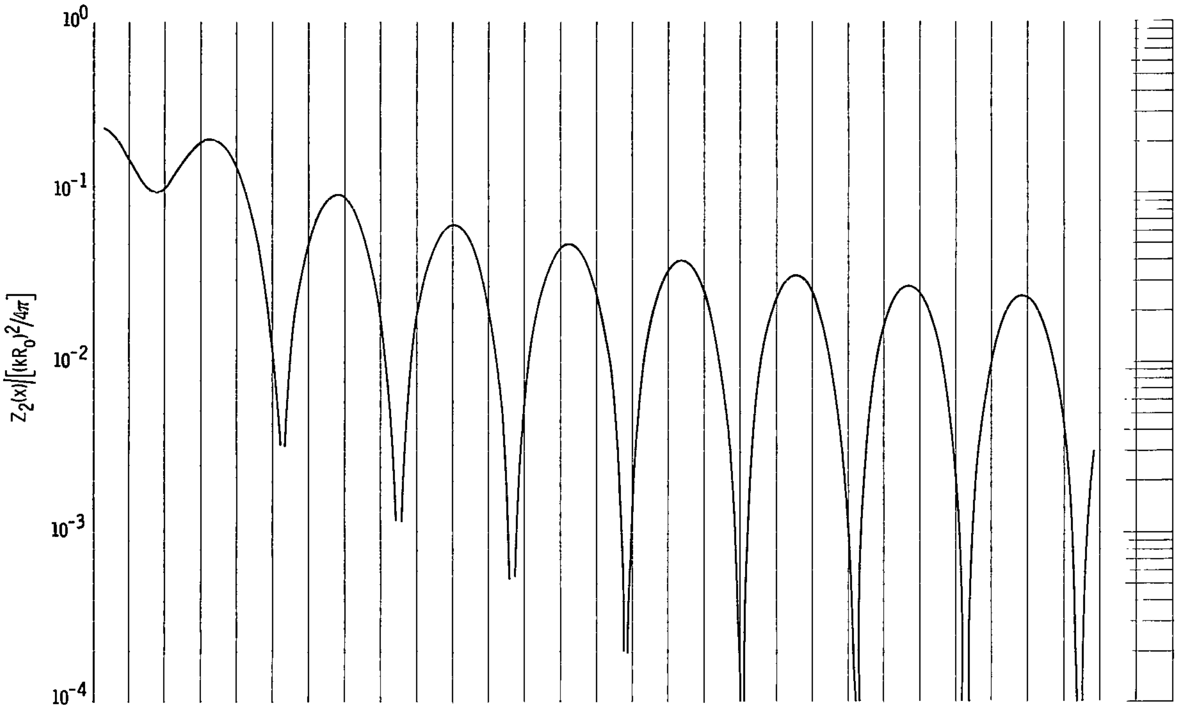

(b) $l = 2$.

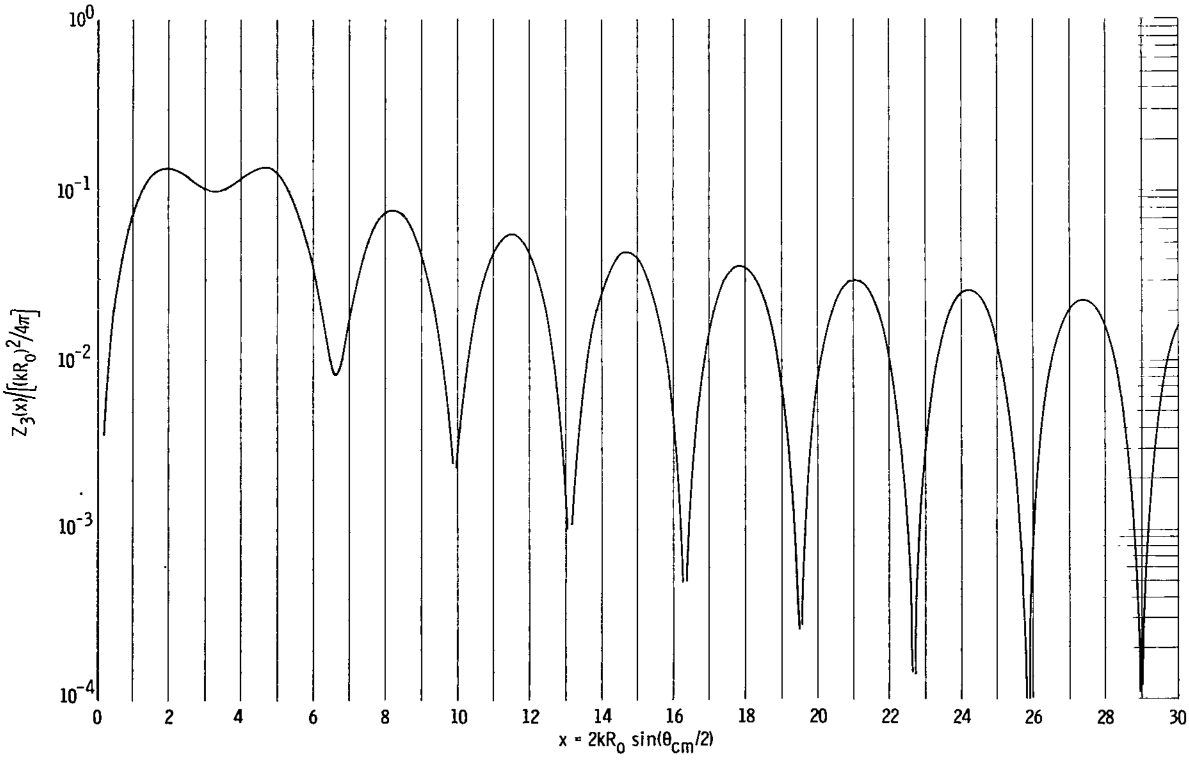

(c) $l = 3$.

Figure 8. - Continued.

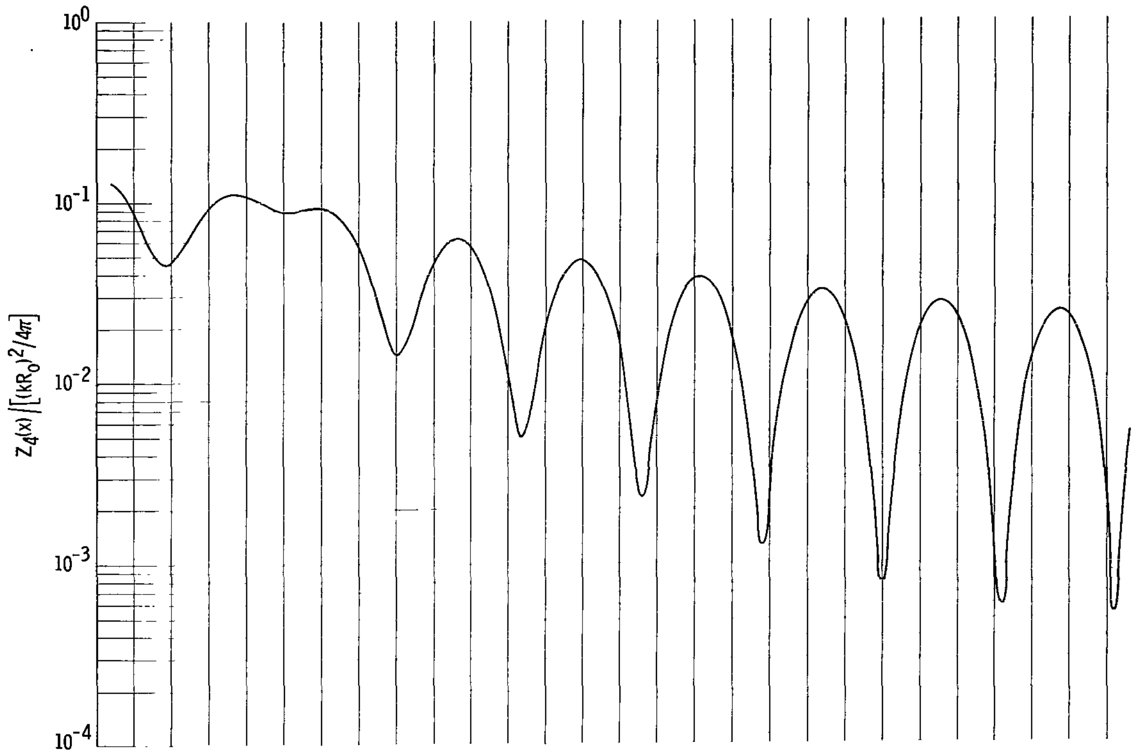

(d) $l = 4$.

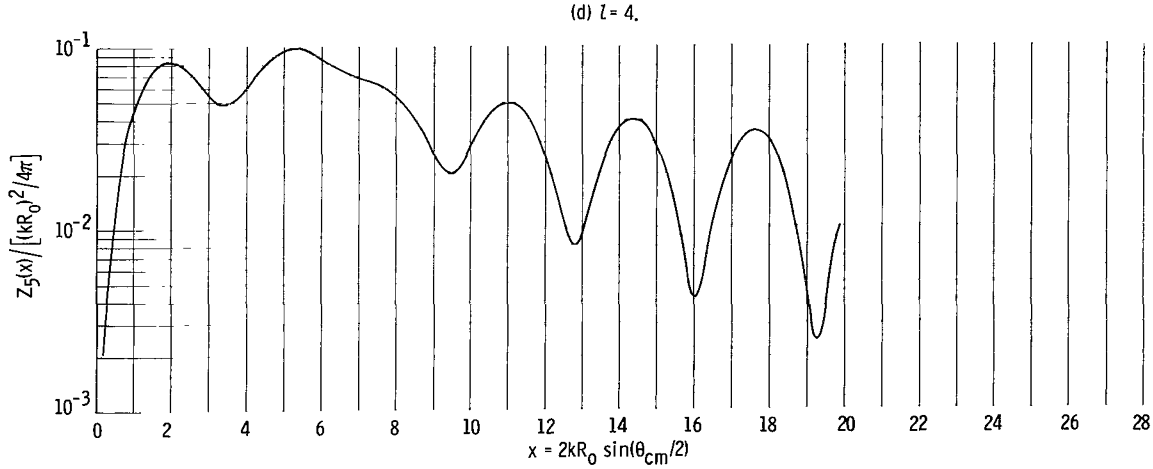

(e) $l = 5$.

Figure 8. - Concluded.

tinguishable for values of $x \geq 10$. The same is seen to be true for angular momentum transfers of 3 and 5.

ANALYSIS OF ELASTIC SCATTERING DATA

Introduction

All four tin isotopes were subjected to the same treatment. Elastic angular distributions were analyzed in terms of an optical model. These results were then used to predict differential cross sections for scattering to each of the excited states, using the DWBA calculation. The data were also analyzed in terms of the Fraunhofer "black disk" model.

Optical Model Fitting

For each of the four elastic angular distributions an optical model analysis was performed (ref. 10). The potential assumed was that defined in equation (3). The form factor used, both for the real and imaginary parts of the potential, was the Woods-Saxon, defined in equation (4). The program varied the parameters V, W, r_o, and a so as to minimize the quantity

$$\chi^2 = \left| \frac{\sigma_{ex} - \sigma_{th}}{\Delta\sigma_{ex}} \right|^2 \tag{24}$$

In practice it was found that attempting simultaneously to optimize all four parameters resulted in incomplete searches and unsatisfactory results. Best fits were finally obtained by fixing r_o and allowing the program to search for optimum values of the other three parameters. By running a series of searches with various fixed values of r_o, it was possible to find a complete set of four parameters which minimized χ^2.

The optical model parameters which gave the best fit to the data are listed in table I, along with the total reaction cross sections calculated according to equation (10). The total reaction cross sections are in good agreement with the values measured by Wilkins (ref. 12). The angular distributions predicted by these optical potentials are compared with the experimental data in figures 4 to 7. However, there were many other sets of optical model parameters which were found to give almost equally satisfactory fits to the experimental data. Several sets of parameters which fit the ^{120}Sn data almost

TABLE I. - RESULTS OF OPTICAL MODEL CALCULATIONS

Tin-isotope target	Strength of real part of nuclear optical potential, V, MeV	Strength of imaginary part of nuclear optical potential, W, MeV	Diffuseness parameter in Woods-Saxon potential, a, fm	Nuclear radius constant, r_0, fm	Total cross section, mb	$R_{optical\ model}$, fm	$R_{Fraunhofer}$, fm
^{116}Sn	60.1	18.7	0.715	1.46	1890	7.86	7.88
^{118}Sn	61.5	26.1	.673	1.46	1896	7.85	7.82
^{120}Sn	58.0	28.0	.712	1.46	1983	7.95	7.98
^{122}Sn	62.1	30.3	.699	1.46	2000	8.06	8.02

TABLE II. - ALTERNATE OPTICAL MODEL PARAMETERS

FOR ^{120}Sn ELASTIC ANGULAR DISTRIBUTION

Strength of real part of nuclear optical potential, V, MeV	Strength of imaginary part of nuclear optical potential, W, MeV	Diffuseness parameter in Woods-Saxon potential, a, fm	Nuclear radius constant, r_0, fm	χ^2 ratio to best fit for ^{120}Sn; parameters listed in table I
316	145	0.710	1.19	4.00
117	48.0	.707	1.36	1.04
103	42.6	.705	1.38	1.03
87.7	38.5	.708	1.40	1.02
66.1	31.1	.710	1.44	1.00
58.0	28.0	.712	1.46	1.00
52.0	24.9	.703	1.48	1.02
43.4	22.5	.710	1.50	1.02

as well as those in table I are shown, together with relative values of χ^2, in table II. In figure 9, the real part of the optical potential is plotted as a function of r for several of the widely varying sets of parameters listed in table II. It may be seen that these potentials, all of which predict very similar elastic angular distributions, are nearly identical beyond a radius of about 8 fermi. This distance may be defined as an effective nuclear radius and is approximately given by

$$R_{optical\ model} = r_0 A^{1/3} + a \tag{25}$$

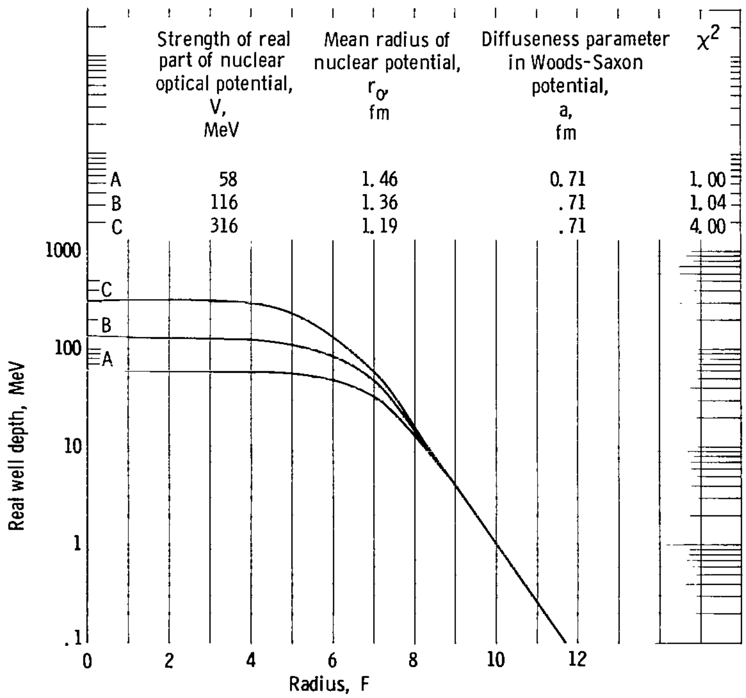

Figure 9. - Real part of alternate optical model potentials for ^{120}Sn.

This quantity is listed for each isotope in table I. This is a vivid illustration of the fact that elastic scattering by tin occurs at the nuclear radius and that the alpha particle is essentially insensitive to the interior details of optical potentials. A similar analysis of optical potential ambiguities was performed by Igo (ref. 13) for alpha scattering from argon, copper, and lead.

Further evidence that the elastic scattering occurs only at the surface, with penetrating particles being absorbed, is gained from an examination of the scattering amplitudes calculated by the optical model program. The reflection coefficient, defined by

$$\left| e^{2i\delta_l} \right| \tag{26}$$

is found to be less than e^{-1} for partial waves of $l \leq 19$, and close to unity for $l > 19$. Hence, waves of $l \leq 19$ are mainly absorbed, while those with $l > 19$ are scattered. Semiclassically, waves of angular momentum l are expected to interact at a radius.

$$r = l/k \tag{27}$$

For $l = 19$ and $k = 2.67\times10^{13}$ cm^{-1}, $r = 19/2.67\times10^{13} = 7.1\times10^{-13}$ cm.

is obtained as the radius at which a division occurs between absorption and scattering. This distance is approximately the effective nuclear radius defined by equation (25).

Fraunhofer Analysis of Elastic Scattering

Using the black disk expression defined by equation (16), it was possible to fit the positions of diffraction peaks in the elastic distributions. Each fit yielded a value of the nuclear radius within which the nucleus is totally absorbing. These radii are listed in table I, under $R_{Fraunhofer}$. It should be noted that they are very nearly equal to the effective nuclear radius obtained from the optical model fits.

Conclusions

From the evidence that the effective nuclear radius is about 8 fermi, that different nuclear potentials produce the same elastic scattering provided they are similar beyond 8 fermi, and that the main contributions to the elastic scattering are those partial waves having $l > 19$, one may conclude that the tin nucleus is strongly absorbing for 40 MeV alpha particles; and the elastic scattering results only from surface reactions of a direct nature.

ANALYSIS OF INELASTIC SCATTERING DATA

Excitation Energies

Using the method outlined in the section Electronics, the excitation energies of both excited states were determined for each isotope. The results are shown in table III. The excitation energies are in good agreement with previously determined values in each case (refs. 14 and 15). The new value of 1.293±0.0008 MeV for the first excited state of ^{116}Sn reported by the Nuclear Data Group of Oak Ridge National Laboratory is acknowledged.

Spin and Parity Detemminations

In figures 4 to 7 it may be observed that the angular distribution of the first excited state in each target is 180 degrees out of phase with the elastic angular distribution to

TABLE III. - SUMMARY OF RESULTS ON ANALYSIS OF INELASTIC SCATTERING

Tin-isotope target	Excitation energy of first excited state, MeV	J^π	Distorted wave Born approximation deformation parameter, β_{DWBA}	Fraunhofer deformation parameter, $\beta_{Fraunhofer}$	Excitation energy of second excited state, MeV	J^π	Distorted wave Born approximation deformation parameter, β_{DWBA}
^{116}Sn	1.287	2^+	0.13±.04	0.11	2.325	3^-	0.15±.03
^{118}Sn	1.207	2^+	.10±.02	----	2.359	3^-	.15±.03
^{120}Sn	1.176	2^+	.12±.02	.12	2.410	3^-	.14±.03
^{122}Sn	1.123	2^+	.13±.03	.10	2.454	3^-	.14±.03

90 degrees. Also, the angular distribution of the second excited state in each target is in phase with the elastic angular distribution to 90 degrees. It is interesting to note that the magnitudes of the first and second excited state cross sections are very similar. Assuming the validity of the Blair phase rule (ref. 1) for transitions to single phonon states, the first excited state must be either a 2^+ or 4^+ level, and the second excited state must be either a 3^- or 5^- level. Of course, it is known that the first strongly excited collective state of tin is 2^+ (ref. 14) and it is expected that the second state is 3^-. However, the second observed state could result from a two-phonon 0^+, 2^+, or 4^+ transition which would also be in phase with the elastic distribution. From analyses by Saudinos (ref. 16) of 44 MeV alpha-particle scattering in the iron-nickel region, the 3^- cross sections are found to be slightly smaller than the 2^+ cross sections. In addition, cross sections for two-phonon transitions were found to be smaller by an order of magnitude than the 3^- cross sections. From the large cross-section ratio of the second excited state to the 2^+ state in tin, it is concluded that this is a transition to a single-phonon 3^- level. This is in agreement with the assignment made by Hansen and Nathan (ref. 15) on the basis of alpha-gamma correlation studies and the inelastic deuteron scattering work of Jolly, Lin, and Cohen (ref. 17). They observed that the Blair phase rule did not hold for the inelastic scattering of 15 MeV deuterons by tin. Thus, it is seen that the angular distributions of elastic and inelastic scattering of 40 MeV alpha particles by even tin isotopes follow very closely the prediction of the Blair phase rule; namely that inelastic distributions of odd momentum transfers are in phase with elastic distributions and out of phase with inelastic distributions of even momentum transfers, for excitations to single phonon states.

Distorted Wave Born Approximation Calculations

An attempt was made to predict the correct angular distributions, assuming transitions to single phonon states. A distorted waves calculation was carried out, using the DRC code (ref. 18). The optical model parameters listed in table I, p. 28 were used to generate both the initial and final distorted waves. The calculation utilized that part of the code concerned with inelastic scattering and employed a surface interaction to cause transitions.

Typically, the single phonon 2^+ and 4^+ calculations resulted in similar angular distributions for $\theta \geq 30^o$, but differed considerably forward of 30^o. The same was true for the single phonon 3^- and 5^- calculations. The 2^+ and 3^- calculations, for the first and second excited states respectively, are clearly in better agreement with the experimental distributions. These calculations are compared with the experimental data in figures 4 to 7.

By normalizing the calculated angular distributions to the experimental data, values of the deformation parameter β_l are obtained. The average value of β_l obtained for each excited state is listed in table III, under the heading β_{DWBA}.

Fraunhofer Treatment of Inelastic Scattering

In addition to the distorted waves analysis, an attempt was made to treat the inelastic data by Fraunhofer scattering from a black disk. Attempts to determine the deformation parameters for the 2^+ states by normalizing to the Fraunhofer prediction for the most forward experimental peak were satisfactory only for ^{116}Sn, ^{120}Sn, and ^{122}Sn; the data for ^{118}Sn were not carried far enough forward to give a suitable peak for normalizing. These Fraunhofer deformation parameters $\beta_{Fraunhofer}$ are also listed in table III.

Reduced Transition Probabilities

The collective nuclear model relates the nuclear deformation to a more directly observable quantity, the reduced transition probability $B(El)$ for electromagnetic excitation of a one phonon state. $B(El)\uparrow$ is given by the equation (ref. 19)

$$B(El)\uparrow = \frac{3}{4\pi}\left(zeR_0^l\right)^2\beta_l^2 \tag{28}$$

TABLE IV. - SUMMARY OF REDUCED TRANSITION PROBABILITIES

Tin isotope	$B(E2)\uparrow_{DWBA}$ ($\times 10^{-49}$ e^2 cm^4)	$B(E2)\uparrow_{Coulomb\ Excitation}$ (ref. 21) ($\times 10^{-49}$ e^2 cm^4)	$\frac{B(E2)\uparrow_{DWBA}}{B(E2)\uparrow_{Single\ Particle}}$
First excited state; $J^\pi = 2^+$			
^{116}Sn	2.83±1.7	2.07	16.8
^{118}Sn	1.72±0.69	2.28	9.9
^{120}Sn	2.52±0.42	2.20	14.3
^{122}Sn	3.02±1.4	2.52	16.8
^{124}Sn	---------	2.13	----
Second excited state; $J^\pi = 3^-$			
Tin isotope	$B(E3)\uparrow_{DWBA}$ ($\times 10^{-74}$ e^2 cm^6)	$B(E3)\uparrow_{Coulomb\ Excitation}$ (ref. 15) ($\times 10^{-74}$ e^2 cm^6)	$\frac{B(E3)\uparrow_{DWBA}}{B(E3)\uparrow_{Single\ Particle}}$
^{116}Sn	12.9±5.2	--	22.9
^{118}Sn	13.4±5.4	--	23.2
^{120}Sn	12.0±5.2	--	20.1
^{122}Sn	12.4±5.3	66	20.0
^{124}Sn	--------	60	----

The quantity $B(El)\uparrow$ may be measured directly in scattering experiments at energies below the Coulomb barrier (ref. 20). The values of $B(E2)\uparrow$ and $B(E3)\uparrow$ obtained in the present experiment are shown in table IV under the headings $B(E2)\uparrow_{DWBA}$ and $B(E3)\uparrow_{DWBA}$.

Also listed in table IV are $B(E2)\uparrow$ values measured by Stelson and McGowan (ref. 21) and two $B(E3)\uparrow$ values, measured by Hansen and Nathan (ref. 15). These measurements were made with Coulomb excitation and are listed under the headings $B(E2)\uparrow_{Coulomb\ excitation}$ and $B(E3)\uparrow_{Coulomb\ excitation}$.

Also shown in table IV is the ratio of measured $B(El)\uparrow$ to the so-called single particle transition rate $B(El)\uparrow_{single\ particle}$. The single particle transition rates are given by

$$B(E2)\uparrow = \frac{5}{4\pi}\left|\frac{3}{5} R_o^2\right|^2 e^2cm^4 \text{ (ref. 21)} \tag{29}$$

$$B(E3)\uparrow = 4.16\ A^2e^2\times10^{-79}\ cm^6 \text{ (ref. 15)} \tag{30}$$

DISCUSSION AND CONCLUSION

Blair Phase Rule

The experimental data demonstrate directly that the Blair phase rule is well followed in alpha-particle scattering at this energy from these isotopes.

Optical Model Analysis

The optical model analysis provides a best-fit potential which is comparable to those usually obtained from this type of experiment. The potential, however, is not unique and others fit the experimental data very nearly as well. The similarity of the outer edges of good potentials, together with the sizes of the phase shifts, and the results of the Fraunhofer analysis all are consistent with the fact that elastic alpha scattering is a surface phenomenon, with more deeply penetrating particles being absorbed (ref. 13).

Distorted Wave Born Approximation Predictions

The DWBA predictions for angular distributions fit the experimental results very well. Predictions based on other spin assignments were sufficiently different at forward angles so that spin assignments could have been made, had they not already been known.

Nuclear Deformations and Reduced Transition Probabilities

The values of the nuclear deformation parameter which are obtained directly from this experiment are quantities defined only within the framework of the collective nuclear model (ref. 19). It is not obvious that experiments of the type reported here should yield the same result as experiments at energies well below the Coulomb barrier. Nevertheless, the agreement between values of $B(E2)\uparrow$ measured by the two methods is very good, somewhat better than is typical (ref. 22). The $B(E3)\uparrow$ values measured here, however, are smaller by about a factor of five than those reported by Hansen and Nathan. However, McGowan et al. (ref. 23) reported $B(E3)\uparrow$ values for ^{110}Cd, ^{112}Cd, ^{114}Cd, ^{116}Cd which are smaller by factors of 3 to 6 than those reported for the same isotopes by Hansen and Nathan in reference 15. Thus the value of the deformation parameter, β_l, obtained from nuclear excitation by inelastic scattering of 40-MeV alpha particles appears to be in agreement with the value obtained from Coulomb excitation experiments.

When compared with single particle rates, the transitions studied here are seen to be enhanced by factors of from 10 to 20, as is typical for transitions of this type which are well known to be due not to excitation of a single nucleon, but rather to collective excitations of the nucleus as a whole.

Lewis Research Center,
National Aeronautics and Space Administration,
Cleveland, Ohio, August 5, 1965.

APPENDIX A

EXPERIMENTAL DIFFERENTIAL CROSS SECTIONS AND ASSOCIATED STATISTICAL COUNTING ERRORS

DIFFERENTIAL CROSS SECTIONS FOR ELASTIC SCATTERING

OF 40 MeV ALPHA PARTICLES BY ^{116}Sn

Scattering angle, θ_{CM}, deg	Differential cross section, $d\sigma/d\Omega$, mb/sr	Scattering angle, θ_{CM}, deg	Differential cross section, $d\sigma/d\Omega$, mb/sr	Scattering angle, θ_{CM}, deg	Differential cross section, $d\sigma/d\Omega$, mb/sr
20.33	3180±12	61.37	1.76±.06	103.60	.00946±.00111
22.39	2240±10	63.40	1.01±.05	105.58	.0174±.0015
24.45	1610±6	65.43	.270±.020	108.56	.0110±.0009
26.52	958±5	67.46	.191±.025	110.53	.00373±.00047
28.58	386±2	69.49	.387±.028	113.50	.000415±.000245
30.64	302±2	71.52	.435±.038	115.47	.00155±.00048
32.70	224±1	73.54	.239±.022	117.44	.00484±.00060
34.76	140±1	75.56	.0959±.0175	118.43	.00558±.00090
36.81	64.8±.5	77.58	.0237±.0048	119.41	.00713±.00077
38.87	43.9±.7	79.59	.0970±.0176	120.40	.00721±.00103
40.92	43.1±.4	81.61	.147±.015	122.36	.00440±.00082
42.98	30.2±.5	83.62	.0925±.0169	124.33	.00194±.00043
45.03	14.8±.2	85.63	.0327±.0054	126.29	.000750±.000221
47.08	7.24±.23	88.64	.0101±.0011	128.25	.000566±.000193
49.12	8.04±.13	90.64	.0242±.0016	129.23	.00102±.00031
51.17	8.09±.24	92.64	.0381±.0028	131.18	.00177±.00038
53.21	5.41±.09	93.64	.0382±.0021	133.14	.00274±.00047
55.25	2.12±.11	98.63	.0108±.0012	136.07	.00216±.00059
57.29	1.25±.05	99.62	.000829±.000424	141.91	.000240±.000100
59.33	2.73±.13	101.61	.00402±.00067		

DIFFERENTIAL CROSS SECTIONS FOR INELASTIC SCATTERING

OF 40 MeV ALPHA PARTICLES BY ^{116}Sn

TO 1.287 MeV LEVEL OF ^{116}Sn

Scattering angle, θ_{CM}, deg	Differential cross section, $d\sigma/d\Omega$, mb/sr	Scattering angle, θ_{CM}, deg	Differential cross section, $d\sigma/d\Omega$, mb/sr	Scattering angle, θ_{CM}, deg	Differential cross section, $d\sigma/d\Omega$, mb/sr
24.47	3.03±.26	44.02	.483±.017	65.46	.180±.020
26.53	10.2±.5	45.05	1.08±.06	67.49	.157±.023
28.59	7.62±.24	47.10	1.21±.09	69.52	.0794±.0127
30.66	4.91±.13	49.15	.696±.039	71.55	.0265±.0092
32.72	1.91±.09	51.19	.178±.040	73.57	.0196±.0058
33.75	1.12±.03	53.24	.300±.021	75.59	.0265±.0092
34.78	1.65±.14	55.28	.510±.053	77.61	.0644±.0081
36.83	4.06±.14	57.32	.506±.033	79.63	.0322±.0104
38.89	2.68±.17	59.36	.337±.047	81.64	.0184±.0046
40.94	1.16±.06	61.40	.0380±.0081	83.65	.00311±.00035
41.97	.514±.020	63.43	.101±.015	85.66	.0161±.0035

DIFFERENTIAL CROSS SECTIONS FOR INELASTIC SCATTERING

OF 40 MeV ALPHA PARTICLES BY ^{116}Sn

TO 2.325 MeV LEVEL OF ^{116}Sn

Scattering angle, θ_{CM}, deg	Differential cross section, $d\sigma/d\Omega$, mb/sr	Scattering angle, θ_{CM}, deg	Differential cross section, $d\sigma/d\Omega$, mb/sr	Scattering angle, θ_{CM}, deg	Differential cross section, $d\sigma/d\Omega$, mb/sr
22.41	7.69±.59	44.04	1.07±.03	63.46	.221±.022
26.54	3.97±.30	45.07	.895±.052	65.49	.0679±.0115
28.61	5.19±.20	46.09	.336±.013	67.52	.0610±.0138
30.67	8.27±.31	47.12	.338±.050	69.55	.102±.015
32.73	4.11±.14	49.17	.531±.022	71.57	.0898±.0173
33.76	2.75±.05	51.21	.626±.021	73.60	.0656±.0115
34.79	2.18±.16	53.26	.567±.029	75.62	.0228±.0081
36.85	1.36±.08	55.30	.226±.035	77.64	.0104±.0035
38.91	1.20±.12	57.34	.155±.018	79.65	.0224±.0069
40.96	2.14±.08	59.38	.246±.040	83.68	.0288±.0092
43.02	1.72±.11	61.42	.260±.024	85.69	.0265±.0046

DIFFERENTIAL CROSS SECTIONS FOR ELASTIC SCATTERING

OF 40 MeV ALPHA PARTICLES BY ^{118}Sn

Scattering angle, θ_{CM}, deg	Differential cross section, $d\sigma/d\Omega$, mb/sr	Scattering angle, θ_{CM}, deg	Differential cross section, $d\sigma/d\Omega$, mb/sr	Scattering angle, θ_{CM}, deg	Differential cross section, $d\sigma/d\Omega$, mb/sr
28.56	501±2	69.46	.466±.012	101.58	.00550±.00059
29.59	398±2	71.48	.510±.020	103.57	.0113±.0008
30.62	342±2	73.51	.362±.011	105.55	.0165±.0016
32.68	264±1	74.52	.217±.013	107.53	.00597±.00044
34.74	166±1	76.54	.0455±.0011	110.50	.000899±.00024
37.82	60.9±.5	77.54	.0504±.0032	114.46	.00338±.00034
39.88	53.0±.6	79.56	.0880±.0057	116.43	.00522±.00043
41.93	53.6±.4	81.57	.134±.003	119.38	.00576±.00083
43.98	28.0±.3	83.58	.109±.006	123.32	.00316±.00034
47.05	9.60±.13	85.59	.0542±.0027	124.30	.00250±.00056
49.10	9.52±.14	86.60	.0362±.0010	125.28	.000912±.000184
51.14	9.54±.11	87.60	.00523±.00123	128.22	.000824±.000267
53.19	6.35±.09	89.60	.0123±.0014	130.18	.00101±.00026
55.23	2.48±.06	91.61	.0229±.0025	132.14	.00251±.00023
56.25	1.88±.04	92.61	.0363±.0144	134.09	.00222±.00024
58.29	1.68±.04	93.60	.0403±.0024	138.97	.000172±.000067
60.32	2.14±.05	94.60	.0326±.0014	140.92	.0000899±.0000412
61.34	2.12±.04	95.60	.0244±.0018	142.87	.0000642±.0000380
63.37	1.27±.04	96.60	.0224±.0013	145.79	.000191±.000079
65.40	.515±.009	98.59	.00631±.00057	147.73	.000632±.000205
67.43	.180±.011	100.58	.00522±.00095	149.67	.000596±.000127
68.45	.337±.007				

DIFFERENTIAL CROSS SECTIONS FOR INELASTIC SCATTERING

OF 40 MeV ALPHA PARTICLES BY ^{118}Sn

TO 1.207 MeV LEVEL OF ^{118}Sn

Scattering angle, θ_{CM}, deg	Differential cross section, $d\sigma/d\Omega$, mb/sr	Scattering angle, θ_{CM}, deg	Differential cross section, $d\sigma/d\Omega$, mb/sr	Scattering angle, θ_{CM}, deg	Differential cross section, $d\sigma/d\Omega$, mb/sr
28.58	3.61±.18	51.17	.336±.019	73.54	.0275±.0029
29.61	3.82±.20	53.21	.266±.017	74.55	.0380±.0054
30.64	4.70±.18	55.25	.486±.023	77.58	.0664±.0036
32.70	1.95±.18	56.27	.560±.019	79.59	.0498±.0043
34.76	1.69±.08	58.31	.346±.019	83.62	.00741±.00155
35.78	3.47±.27	60.35	.129±.012	85.62	.00988±.00119
37.84	4.44±.13	61.37	.0884±.0077	87.63	.0144±.0020
39.89	2.00±.12	63.40	.0904±.0099	89.64	.0166±.0015
41.95	.664±.052	65.43	.182±.005	91.64	.0173±.0022
44.00	1.22±.07	68.48	.156±.005	93.64	.00365±.00070
47.07	1.31±.05	69.49	.113±.006	95.63	.00372±.00070
49.12	.871±.040	71.51	.0296±.0048		

DIFFERENTIAL CROSS SECTIONS FOR INELASTIC SCATTERING

OF 40 MeV ALPHA PARTICLES BY ^{118}Sn

TO 2.359 MeV LEVEL OF ^{118}Sn

Scattering angle, θ_{CM}, deg	Differential cross section, $d\sigma/d\Omega$, mb/sr	Scattering angle, θ_{CM}, deg	Differential cross section, $d\sigma/d\Omega$, mb/sr	Scattering angle, θ_{CM}, deg	Differential cross section, $d\sigma/d\Omega$, mb/sr
28.59	5.96±.23	51.19	.760±.029	73.57	.0938±.0053
29.62	2.90±.18	53.24	.640±.027	74.58	.0501±.0062
30.65	6.01±.20	55.28	.330±.020	77.61	.0281±.0024
32.71	5.57±.19	56.30	.273±.014	79.62	.0204±.0028
34.77	3.98±.12	58.34	.224±.156	83.65	.0374±.0035
35.80	4.38±.30	60.38	.327±.019	85.66	.0255±.0020
37.86	1.54±.08	61.39	.355±.015	86.66	.0215±.0025
39.92	1.69±.10	63.43	.255±.017	89.67	.00974±.00117
41.97	2.65±.08	65.46	.139±.005	91.67	.0107±.0017
44.02	1.54±.07	68.50	.0784±.0035	93.67	.0103±.0012
47.10	.686±.034	69.52	.0841±.0051	95.67	.0140±.0014
49.15	.811±.039	71.54	.101±.009		

DIFFERENTIAL CROSS SECTIONS FOR ELASTIC SCATTERING

OF 40 MeV ALPHA PARTICLES BY ^{120}Sn

Scattering angle, θ_{CM}, deg	Differential cross section, $d\sigma/d\Omega$, mb/sr	Scattering angle, θ_{CM}, deg	Differential cross section, $d\sigma/d\Omega$, mb/sr	Scattering angle, θ_{CM}, deg	Differential cross section, $d\sigma/d\Omega$, mb/sr
18.24	7650±24	65.37	.220±.015	107.50	.00476±.00074
20.30	4010±7	67.40	.263±.016	109.48	.000793±.000308
22.37	2250±1	69.43	.430±.020	111.46	.000230±.000167
24.43	1480±1	71.45	.348±.018	113.44	.00151±.00043
26.49	701±21	73.48	.141±.012	114.43	.00308±.00061
28.55	411±1	75.50	.0461±.0066	115.41	.00496±.00079
30.61	282±1	77.51	.0530±.0071	116.40	.00485±.00077
32.66	209±1	79.53	.0940±.0041	117.38	.00418±.00073
34.72	124±1	82.55	.0787±.0038	118.37	.00328±.00064
36.78	56.7±.3	84.56	.0376±.0026	120.34	.00226±.00053
38.83	42.8±.3	86.56	.00771±.00088	122.31	.000120±.000041
40.88	38.2±.4	88.57	.0161±.0013	124.27	.000124±.000124
42.93	23.9±.3	91.57	.0318±.0018	128.19	.000948±.000294
44.98	13.6±.2	93.57	.0251±.0022	129.17	.00138±.00043
47.03	6.75±.12	95.57	.00983±.00100	133.09	.00136±.00035
49.07	8.41±.13	96.57	.00642±.00081	135.04	.000877±.000285
51.12	7.00±.08	98.56	.000728±.000283	137.00	.000890±.000289
53.61	3.72±.07	100.55	.00468±.00071	141.87	.0000888±.0000888
55.20	1.36±.04	102.54	.00956±.00104	143.82	.000449±.000188
57.24	1.47±.05	103.53	.0107±.0011	145.77	.000685±.000315
59.28	1.90±.05	104.53	.0124±.0014	148.68	.000300±.000154
61.31	1.59±.04	106.51	.00695±.00104	150.63	.000275±.000200
63.34	.675±.026				

DIFFERENTIAL CROSS SECTIONS FOR INELASTIC SCATTERING

OF 40 MeV ALPHA PARTICLES BY ^{120}Sn

TO 1.176 MeV LEVEL OF ^{120}Sn

Scattering angle, θ_{CM}, deg	Differential cross section, $d\sigma/d\Omega$, mb/sr	Scattering angle, θ_{CM}, deg	Differential cross section, $d\sigma/d\Omega$, mb/sr	Scattering angle, θ_{CM}, deg	Differential cross section, $d\sigma/d\Omega$, mb/sr
20.31	29.8±.6	45.00	1.03±.05	67.43	.124±.011
22.38	22.9±.5	47.05	.864±.042	69.46	.0468±.0066
24.44	2.25±.15	49.10	.390±.028	71.48	.00728±.00264
26.50	3.29±.14	51.14	.143±.012	73.50	.0207±.0044
28.56	6.62±.13	53.18	.212±.018	75.52	.0429±.0062
30.62	3.92±.10	55.22	.401±.021	77.54	.0318±.0053
32.68	1.03±.05	57.26	.338±.022	79.56	.0105±.0034
34.74	1.71±.07	59.30	.0778±.0149	81.57	.00517±.00213
36.79	2.95±.08	61.34	.0306±.0054	84.59	.00376±.00213
38.85	2.06±.07	63.37	.0842±.0089	87.60	.0149±.0061
40.90	.790±.041	65.40	.167±.013	91.60	.00483±.00345
42.95	.553±.041				

DIFFERENTIAL CROSS SECTIONS FOR INELASTIC SCATTERING

OF 40 MeV ALPHA PARTICLES BY ^{120}Sn

to 2.410 MeV LEVEL OF ^{120}Sn

Scattering angle, θ_{CM}, deg	Differential cross section, $d\sigma/d\Omega$, mb/sr	Scattering angle, θ_{CM}, deg	Differential cross section, $d\sigma/d\Omega$, mb/sr	Scattering angle, θ_{CM}, deg	Differential cross section, $d\sigma/d\Omega$, mb/sr
20.33	4.16±.21	42.97	1.54±.07	65.43	.0730±.0084
22.39	5.07±.22	45.03	.753±.039	67.46	.0437±.0064
24.45	8.53±.29	47.07	.540±.033	69.49	.0867±.0094
26.52	8.58±.23	49.12	.660±.038	71.51	.0846±.0087
28.58	3.62±.10	51.17	.518±.023	73.54	.0541±.0070
30.64	6.32±.13	53.21	.377±.024	75.56	.0259±.0049
32.70	2.82±.10	55.25	.163±.014	77.58	.0115±.0032
34.76	1.65±.07	57.29	.208±.017	79.59	.0148±.0037
36.81	1.10±.05	59.33	.239±.024	81.61	.0284±.0050
38.87	1.39±.06	61.37	.223±.015	84.62	.00756±.00305
40.92	1.54±.06	63.40	.115±.010		

DIFFERENTIAL CROSS SECTIONS FOR ELASTIC SCATTERING

OF 40 MeV ALPHA PARTICLES BY ^{122}Sn

Scattering angle, θ_{CM}, deg	Differential cross section, $d\sigma/d\Omega$, mb/sr	Scattering angle, θ_{CM}, deg	Differential cross section, $d\sigma/d\Omega$, mb/sr	Scattering angle, θ_{CM}, deg	Differential cross section, $d\sigma/d\Omega$, mb/sr
20.29	4320±11	61.28	1.55±.06	104.50	.0136±.0015
22.35	1840±7	63.32	.652±.034	106.48	.00803±.00131
24.41	1650±5	65.35	.275±.022	109.45	.000420±.000238
26.47	843±3	67.37	.403±.026	111.43	.00112±.00048
28.53	423±2	69.40	.528±.030	113.41	.00301±.00081
30.59	322±2	71.42	.351±.024	115.38	.00466±.00083
32.65	242±1	73.45	.124±.012	118.34	.00555±.00110
34.70	129.0±.9	75.47	.0496±.0106	120.31	.00182±.00052
36.76	67.5±.4	77.48	.0981±.0060	122.28	.000708±.000354
38.81	51.4±.4	79.50	.160±.008	124.24	.000119±.000119
40.86	47.7±.4	82.52	.0778±.0050	127.19	.000474±.000237
42.91	27.7±.3	84.53	.0279±.0030	129.15	.00228±.00059
44.96	13.5±.2	86.53	.0128±.0015	131.11	.00210±.00058
47.01	9.03±.17	88.54	.0267±.0023	133.07	.00125±.00045
49.05	10.3±.2	91.54	.0334±.0024	136.00	.000496±.000248
51.09	7.85±.15	93.54	.0196±.0019	141.85	.000388±.000254
53.14	3.59±.10	95.54	.00928±.00140	144.77	.000515±.000257
55.18	1.57±.05	97.53	.000748±.000379	146.72	.00104±.00042
57.21	1.91±.07	100.52	.00907±.00130	148.67	.000272±.000191
59.25	2.12±.07	102.51	.0134±.0016		

DIFFERENTIAL CROSS SECTIONS FOR INELASTIC SCATTERING

OF 40 MeV ALPHA PARTICLES BY ^{122}Sn

TO 1.123 MeV LEVEL OF ^{122}Sn

Scattering angle, θ_{CM}, deg	Differential cross section, $d\sigma/d\Omega$, mb/sr	Scattering angle, θ_{CM}, deg	Differential cross section, $d\sigma/d\Omega$, mb/sr	Scattering angle, θ_{CM}, deg	Differential cross section, $d\sigma/d\Omega$, mb/sr
20.30	24.2±.8	40.88	.928±.055	59.27	.0915±.0129
22.36	3.62±.20	41.90	1.03±.08	61.31	.0816±.0122
25.46	4.05±.46	42.93	.900±.054	63.34	.124±.014
27.52	8.44±.65	44.98	1.18±.05	65.37	.186±.017
30.60	4.19±.17	47.03	1.02±.05	67.40	.118±.013
32.66	1.46±.12	49.07	.384±.043	69.43	.0289±.0063
34.72	2.21±.18	51.12	.191±.022	71.45	.0159±.0048
36.77	2.94±.13	53.16	.423±.031	73.47	.0340±.0168
37.80	2.77±.17	55.20	.500±.028	75.49	.0482±.0098
38.83	2.19±.08	57.24	.302±.027		

DIFFERENTIAL CROSS SECTIONS FOR INELASTIC SCATTERING

OF 40 MeV ALPHA PARTICLES BY ^{122}Sn

TO 2.454 MeV LEVEL OF ^{122}Sn

Scattering angle, θ_{CM}, deg	Differential cross section, $d\sigma/d\Omega$, mb/sr	Scattering angle, θ_{CM}, deg	Differential cross section, $d\sigma/d\Omega$, mb/sr	Scattering angle, θ_{CM}, deg	Differential cross section, $d\sigma/d\Omega$, mb/sr
25.47	10.9±.8	42.95	1.23±.06	61.34	.214±.020
27.53	4.65±.49	45.00	.779±.043	63.37	.108±.013
30.62	6.02±.20	47.05	.544±.039	65.40	.0788±.0110
32.68	5.76±.23	49.10	.677±.037	67.43	.0442±.0080
34.74	1.92±.17	51.14	.459±.035	69.46	.0613±.0094
36.79	1.48±.09	53.19	.371±.030	71.49	.0670±.0094
38.85	1.37±.07	55.23	.225±.019	73.51	.0435±.0076
40.90	1.51±.07	57.27	.207±.022	75.53	.0181±.0060
41.93	1.68±.14	59.30	.236±.020		

REFERENCES

1. Blair, John S.: Inelastic Diffraction Scattering. Phys. Rev., vol. 115, no. 4, Aug. 15, 1959, pp. 928-938.
2. Glendenning, Norman K.: Theory of Direct-Interaction Inelastic Scattering. Phys. Rev., vol. 114, no. 5, June 1, 1959, pp. 1297-1311.
3. Rost, E.; and Austern, N.: Inelastic Diffraction Scattering. Phys. Rev., vol. 120, no. 4, Nov. 15, 1960, pp. 1375-1387.
4. Bassel, R. H.; Satchler, G. R.; Drisko, R. M.; and Rost, E.: Analysis of the Inelastic Scattering of Alpha Particles. I. Phys. Rev., vol. 128, no. 6, Dec. 15, 1962, pp. 2693-2707.
5. Rost, E.: Analysis of the Inelastic Scattering of Alpha Particles. II. Phys. Rev., vol. 128, no. 6, Dec. 15, 1962, pp. 2708-2716.
6. Cohen, Bernard L.: Resolution of Accelerator Magnetic Analyzing Systems. Rev. Sci. Inst., vol. 30, no. 6, June 1959, pp. 415-418.
7. Cohen, Bernard L.: Limitations of Accelerator Magnetic Analyzing Systems. Rev. Sci. Inst., vol. 33, no. 1, Jan. 1962, pp. 85-92.
8. Anon.: Cyclotron Research. Annual Prog. Rept., Univ. Wash., 1962, pp. 46-47.
9. Williamson, C.; and Boujot, J. P.: Tables of Range and Rate of Energy Loss of Charged Particles of Energy 0.5 to 150 Mev. Rept. No. CEA-2189, Centre d'Etudes Nucléaires, Saclay, 1963.
10. Melkanoff, Michel A.; Nodvik, John S.; Saxon, David S.; and Cantor, David G.: A FORTRAN Program for Elastic Scattering Analyses with the Nuclear Optical Model. Univ. Calif. Press, 1961.
11. Hodgson, P. E.: The Optical Model of Elastic Scattering. Oxford Univ. Press, 1963.
12. Wilkins, Bruce D.: Total-Reaction Cross-Section Measurements for Charged Particles. Rept. No. UCRL 10783, AEC, May 9, 1963.
13. Igo, George: Optical-Model Analysis of Excitation Function Data and Theoretical Reaction Cross Sections for Alpha Particles. Phys. Rev., vol. 115, no. 6, Sept. 15, 1959, pp. 1665-1674.
14. Nuclear Data Group: Nuclear Data Sheet Nos. NRC-60-3-117; 60-3-140; 60-4-66; and 60-4-85. Oak Ridge Nat. Lab., 1965.
15. Hansen, O.; and Nathan, O.: Excitation of Collective Octupole States in the Pd-Sm Region. Nucl. Phys., vol. 42, no. 2, Apr. 1963, pp. 197-220.

16. Saudinos, Jean: Nouveaux Aspects de l'excitation nucléaire par diffusion de particules alpha. (New Features of Nuclear Excitation by α Particles Scattering.) Rept. No. CEA-2146, Centre d'Études Nucléaires, Saclay, 1962.

17. Jolly, R. K.; Lin, E. K.; and Cohen, B. L.: Studies of 15-MeV Inelastic Deuteron Scattering. Phys. Rev., vol. 128, no. 5, Dec. 1, 1962, pp. 2292-2302.

18. Gibbs, W. R.; Madsen, V. A.; Miller, J. A.; Tobocman, W.; Cox, E. C.; and Mowry, L.: Direct Reaction Calculation. NASA TN D-2170, 1964.

19. Nathan, O.; and Nilsson, S. G.: Collective Nuclear Motion and the Unified Model. Vol. I of Alpha-, Beta- and Gamma-Ray Spectroscopy, K. Siegbahn, ed., North-Holland Pub. (Amsterdam), 1965, pp. 601-700.

20. Alder, K.; Bohr, A.; Huus, T.; Mottelson, B.; and Winther, A.: Study of Nuclear Structure by Electromagnetic Excitation with Accelerated Ions. Rev. Modern Phys., vol. 28, no. 4, Oct. 1956, pp. 432-542.

21. Stelson, P. H.; and McGowan, F. K.: Coulomb Excitation of Medium-Weight Even-Even Nuclei. Phys. Rev., vol. 110, no. 2, Apr. 15, 1958, pp. 489-506.

22. Faraggi, H.; and Saudinos, J.: Spectroscopic Data Deduced from Inelastic Scattering of 44-Mev Alpha Particles in Medium Weight Nuclei. Nuclear Spectroscopy with Direct Reactions. I - Contributed Papers. Rept. No. ANL 6848, F. E. Throw, ed., Mar. 1964, pp. 137-142.

23. McGowan, F. K.; Robinson, R. L.; Stelman, P. H.; Ford, J. L. C.; and Milner, W. T.: Coulomb Excitation of Vibrational Triplet States and Octupole States in the Even Cadmium Nuclei. Bull. Am. Phys. Soc., ser. II, vol. 9, no. 1, 1964, p. 107.

24. Bohr, A.; and Mottelson, B. R.: Collective and Individual-Particle Aspects of Nuclear Structure. K. Danske Uidensk. Selsk. mat.-fys. Medd., vol. 27, no. 16, 1953.

3/12/85

"The aeronautical and space activities of the United States shall be conducted so as to contribute . . . to the expansion of human knowledge of phenomena in the atmosphere and space. The Administration shall provide for the widest practicable and appropriate dissemination of information concerning its activities and the results thereof."

—NATIONAL AERONAUTICS AND SPACE ACT OF 1958

NASA SCIENTIFIC AND TECHNICAL PUBLICATIONS

TECHNICAL REPORTS: Scientific and technical information considered important, complete, and a lasting contribution to existing knowledge.

TECHNICAL NOTES: Information less broad in scope but nevertheless of importance as a contribution to existing knowledge.

TECHNICAL MEMORANDUMS: Information receiving limited distribution because of preliminary data, security classification, or other reasons.

CONTRACTOR REPORTS: Technical information generated in connection with a NASA contract or grant and released under NASA auspices.

TECHNICAL TRANSLATIONS: Information published in a foreign language considered to merit NASA distribution in English.

TECHNICAL REPRINTS: Information derived from NASA activities and initially published in the form of journal articles.

SPECIAL PUBLICATIONS: Information derived from or of value to NASA activities but not necessarily reporting the results of individual NASA-programmed scientific efforts. Publications include conference proceedings, monographs, data compilations, handbooks, sourcebooks, and special bibliographies.

Details on the availability of these publications may be obtained from:

SCIENTIFIC AND TECHNICAL INFORMATION DIVISION

NATIONAL AERONAUTICS AND SPACE ADMINISTRATION

Washington, D.C. 20546